

RICE UNIVERSITY

**Laurentide Ice Sheet Meltwater Influences and Millennial-Scale
Climate Oscillations on the Northwestern Slope of the Gulf of Mexico
During Marine Isotope Stage 6 and Termination II**


By

Walter Werley O'Hayer


A THESIS SUBMITTED
IN PARTIAL FULFILLMENT OF THE
REQUIREMENTS FOR THE DEGREE

Master of Science


APPROVED, THESIS COMMITTEE:



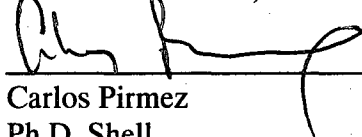
André W. Droxler, Co-Chair
Professor, Earth Science



Brandon Dugan, Co-Chair
Assistant Professor, Earth Science



Caroline A. Masiello
Assistant Professor, Earth Science



Carlos Pirmez
Ph.D, Shell

HOUSTON, TEXAS

MAY 2009

UMI Number: 1466813

INFORMATION TO USERS

The quality of this reproduction is dependent upon the quality of the copy submitted. Broken or indistinct print, colored or poor quality illustrations and photographs, print bleed-through, substandard margins, and improper alignment can adversely affect reproduction.

In the unlikely event that the author did not send a complete manuscript and there are missing pages, these will be noted. Also, if unauthorized copyright material had to be removed, a note will indicate the deletion.

UMI[®]

UMI Microform 1466813
Copyright 2009 by ProQuest LLC
All rights reserved. This microform edition is protected against
unauthorized copying under Title 17, United States Code.

ProQuest LLC
789 East Eisenhower Parkway
P.O. Box 1346
Ann Arbor, MI 48106-1346

ABSTRACT

Laurentide Ice Sheet Meltwater Influences and Millennial-Scale Climate Oscillations on the Northwestern Slope of the Gulf of Mexico During Marine Isotope Stage 6 and Termination II

by

Walter Werley O'Hayer

Sub-Milankovitch climate oscillations are well documented phenomena in the Gulf of Mexico during Marine Isotope Stage (MIS) 3 and Termination I, however very little is known about equivalent events during older time intervals. Basin 4 is located on the northwest slope of the Gulf of Mexico and has provided a detailed record of late MIS 6 and Termination II. The results of this study show that the $\delta^{18}\text{O}$ record of planktonic foraminifer *G. ruber* contains millennial-scale climate oscillations during MIS 6, a series of meltwater spikes, and a climate reversal during Termination II. Paired $\delta^{18}\text{O}$ – Mg/Ca data across these events reveal that the unusually large amplitudes in the $\delta^{18}\text{O}$ record cannot be explained by sea surface temperature (SST) or ice volume, but rather are a response to isotopically light glacial meltwater from the paleo-Mississippi river. This conclusion supports the studies of similar oscillations during Termination I and MIS 3.

ACKNOWLEDGEMENTS

I would like to thank my co-advisors Dr. André Droxler and Dr. Brandon Dugan for their support and guidance during my time at Rice. Their insight and advice has made me a better scientist and has helped prepare me for future challenges. Many thanks to my thesis and proposal committee, including Dr. Caroline Masiello, Dr. Carlos Pirmez, and Dr. Laurent Labeyrie. Special thanks to the Department of Earth Science staff who helped me during my numerous teaching assistantships.

This research used samples and data provided by IODP. Funding was provided by a JOI USSAC grant. I would like to thank the collaborators at the Laboratoire des Sciences du Climat et de l'Environnement, CNRS, Gif Sur Yvette, France for their help in processing samples and providing insight into my study area. I would also like to thank those at Processus et Bilans des Domaines Sédimentaires, Université de Lille for providing data on additional cores.

TABLE OF CONTENTS

ABSTRACT.....	ii
ACKNOWLEDGEMENTS.....	iii
TABLE OF CONTENTS.....	iv
LIST OF TABLES.....	vi
LIST OF FIGURES.....	vii
GENERAL INTRODUCTION.....	viii
CHAPTER 1.	1
Abstract.....	1
1.1. Introduction.....	2
1.2. Regional Setting.....	4
1.3. Basin 4 Sediment Sequences.....	5
1.4. Methods.....	6
1.4.1. Stable Isotopes and Mg/Ca.....	6
1.4.1.1. Holes 1319A and 1320A.....	6
1.4.2. Ash Layer and <i>G. menardii</i> Complex.....	8
1.4.3. Mg/Ca Derived SST and $\delta^{18}\text{O}_{\text{seawater}}$ Calculations.....	8
1.4.4. Discussion of $\delta^{18}\text{O}$	9
1.4.5. Discussion of Mg/Ca Method.....	10
1.5 Biostratigraphy and Time Markers.....	11
1.6 Basin 4 $\delta^{18}\text{O}$ Records.....	13
1.6.1. Hole 1319A.....	13

1.6.2. Hole MD03-2641.....	13
1.6.3. Hole 1320A.....	15
1.7. Mg/Ca and Related Records.....	15
1.8. Discussion.....	17
1.8.1. Termination II Meltwater Pulse.....	17
1.8.2. Termination II Reversal.....	20
1.8.3. MIS 6/W1 Interstadial.....	23
1.9. Conclusions.....	25
REFERENCES.....	27
FIGURES.....	33
APPENDIX A. $\delta^{18}\text{O}$ and $\delta^{13}\text{C}$ Records For Basin 4 Cores.....	47
APPENDIX B. Mg/Ca and Related Data for 1319A.....	53
APPENDIX C. Additional Figures.....	56

LIST OF TABLES**CHAPTER 1**

Table 1	Basin 4 Core Locations and Descriptions.....	36
---------	--	----

APPENDIX A.

Table A.1.	Data for Hole 1319A.....	48
------------	--------------------------	----

Table A.2.	Data for Hole 1320A.....	50
------------	--------------------------	----

Table A.3.	Data for MD03-2641.....	51
------------	-------------------------	----

APPENDIX B

Table B.1.	Mg/Ca Data for Hole 1319A.....	54
------------	--------------------------------	----

LIST OF FIGURES

CHAPTER 1

Figure 1.1. Gulf of Mexico Location Map.....	33
Figure 1.2. Late Pleistocene Paleogeographic Map (GoM).....	34
Figure 1.3. Basin 4 Bathymetric Map.....	35
Figure 1.4a. $\delta^{18}\text{O}$ records for Basin 4.....	37
Figure 1.4b. $\delta^{18}\text{O}$ records for Basin 4 (depth corrected).....	38
Figure 1.5. $\delta^{18}\text{O}$ Termination II Climate Reversal.....	39
Figure 1.6. $\delta^{18}\text{O}$ Hole 1319A with Five-point Average and Interpretation.....	40
Figure 1.7. $\delta^{18}\text{O}$ Hole MD03-2641.....	41
Figure 1.8. MIS 6/TII climate proxy records from Hole 1319A.....	42
Figure 1.9. Termination I and II $\delta^{18}\text{O}$ Meltwater Responses in the GoM.....	43
Figure 1.10. $\delta^{18}\text{O}_{\text{sw}}$ and SST curves for TII and TI.....	44
Figure 1.11. $\delta^{18}\text{O}_{\text{sw}}$ and SST curves for MIS 6 and MIS 3.....	45
Figure 1.12. $\delta^{18}\text{O}$ from Basin 4 MIS 6 and MIS 3.....	46

APPENDIX C

Figure C.1. Hole 1319A d18O and d13C.....	57
Figure C.2. Hole 1319A d18O and Average Plots.....	58
Figure C.3. Global Benthic Stack with <i>G. menardii</i> Zones and Age.....	59

GENERAL INTRODUCTION

Millennial-scale climate oscillations have been described, especially for the last 100 ka (Dansgaard et al., 1993; Alley et al., 2000), however the forcing mechanisms behind these cycles are not as well understood as those causing Milankovitch-scale changes. With the aid of ^{14}C dating as well as correlation to high resolution climate records of Greenland and Antarctic ice cores, the timing and magnitude of these rapid climate changes of the last 40 ka are well constrained (Hill et al., 2006).

The Gulf of Mexico (GoM) is particularly sensitive to changes in the Laurentide Ice Sheet (LIS) during these rapid climate changes, as glacial meltwater is routed through the Mississippi (Leventer et al., 1982). The meltwater subsequently changes the isotopic composition of the surface waters, registering a response in the tests of planktonic foraminifers (Flower and Kennett, 1990). These meltwater pulses have been noted for both Marine Isotope Stage (MIS) 3 (Hill et al., 2006) as well as the last deglaciation (Flower et al., 2004) in the Gulf of Mexico. Millennial-scale climate oscillations have also been noted for the penultimate glaciation/deglaciation (MIS 6 / Termination II; Cannariato and Kennett, 2005 and references herein), although lack of a viable dating method for these records, as well as the lack of a northern hemisphere ice record with which to correlate, inhibits a chronology as precise as those for the rapid climate oscillations seen during the last deglaciation and MIS 3.

This study focuses on Basin 4, located on the northwest slope of the GoM, in order to understand millennial-scale climate oscillations seen during MIS 6 and Termination II. Two cores from this basin allow us to constrain the timing of these

millennial-scale oscillations with changes in the Laurentide Ice Sheet, as seen in the $\delta^{18}\text{O}$ record of planktonic foraminifers. A coupling of $\delta^{18}\text{O}$ and Mg/Ca measurements on the planktonic foraminifers allows us to differentiate changes in sea surface temperature and the isotopic composition of the surface waters in the Gulf of Mexico. Ultimately, this research aims to establish the existence of meltwater events during MIS 6 and Termination II in the GoM and suggest that these records can be used to associate the growth and decay cycles of the Laurentide Ice Sheet (LIS) with worldwide records of millennial-scale oscillations during this time period.

CHAPTER 1. Laurentide Ice Sheet Meltwater Influences and Millennial-Scale Climate Oscillations on the Northwestern Slope of the Gulf of Mexico During Marine Isotope Stage 6 and Termination II

Abstract

Sub-Milankovitch climate oscillations are well documented phenomena in the Gulf of Mexico during Marine Isotope Stage (MIS) 3 and Termination I, however very little is known about equivalent events during older time intervals. Basin 4 is located on the northwest slope of the Gulf of Mexico and has provided a detailed record of late MIS 6 and Termination II. The results of this study show that the $\delta^{18}\text{O}$ record of planktonic foraminifer *G. ruber* contains millennial-scale climate oscillations during MIS 6, a series of meltwater spikes, and a climate reversal during Termination II. Paired $\delta^{18}\text{O}$ – Mg/Ca data across these events reveal that the unusually large amplitudes in the $\delta^{18}\text{O}$ record cannot be explained by sea surface temperature (SST) or ice volume, but rather are a response to isotopically light glacial meltwater from the paleo-Mississippi river. This conclusion supports the studies of similar oscillations during Termination I and MIS 3.

1.1 Introduction

Milankovitch scale climate forcing is a well documented phenomena (Hays et al., 1976; Imbrie et al., 1984), however climate records spanning the last 100 ky are punctuated by sub-Milankovitch, millennial-scale climate oscillations such as Dansgaard-Oeschger (D/O) cycles seen in Marine Isotope Stage 3 (MIS 3) and the Bölling-Allerød and Younger Dryas events of the Termination I (TI) (Dansgaard et al., 1993; Alley et al., 2000; Flower et al., 2004). Along with accompanied changes of 8-16 °C in the air temperature in Greenland (Landais et al., 2004; Huber et al., 2006), D/O cycles are important because sea level has been shown to rise and fall by up to 30 m during these rapid events (Lambeck and Chappell, 2001; Siddall et al., 2003). Studies of D/O cycles during the second half of MIS 3 can be anchored by ^{14}C dating, and therefore, correlated to Greenland or Antarctic ice core records (Hill et al., 2006)

The detailed structure of late Marine Isotope Stage 6 (MIS 6) and Termination II (TII) has been extensively studied, and analogues for many of the millennial-scale climate changes of the last deglaciation, such as the Younger Dryas, and D/O cycles in MIS 3, are already described during the previous glacial cycle (Cannariato and Kennett, 2005; Siddall et al., 2007 and references therein). The lack of a viable dating method for many of these records, outside of U/Th used in coral records, as well as commonly low sedimentation rates that prohibit the detailed analyses of these millennial-scale cycles, makes MIS 6 and TII particularly challenging time intervals for the analysis of rapid climate changes.

Studies attempt to correlate foraminiferal marine $\delta^{18}\text{O}$ records of MIS 6 and TII to the Greenland ice cores (Rasmussen et al., 1999), however the bottom of the GRIP ice

record (Johnsen et al., 1997) has problems such as folding, missing section, and inserted layers in the ice record older than MIS 5.5 (Chappellaz et al., 1997). With no ice record in the Northern Hemisphere representing the MIS 6/TII interval, it is almost impossible to establish or discredit a link between ice volume changes in the Laurentide Ice Sheet (LIS) and the changes seen in the records from around the world. The northern Gulf of Mexico (GoM) planktonic foraminifer $\delta^{18}\text{O}$ records from small anoxic basins, such as the Orca Basin, have been shown to be particularly sensitive to rapid changes in the LIS through the routing of isotopically light meltwater through the paleo-Mississippi River (Kennett et al., 1975; Kennett et al., 1985; Leventer et al., 1982; Flower and Kennett, 1990; Figure 1.1).

Meltwater timing and intensity have been studied, using paired Mg/Ca and $\delta^{18}\text{O}$ records, for the last deglaciation (Flower et al., 2004), as well as during MIS 3 abrupt climate changes (Hill et al., 2006). MIS 3-type climate oscillations are postulated to exist during late MIS 6 in Santa Barbara Basin offshore Central California (Cannariato and Kennett, 2005), however a paucity of planktonic foraminifera prohibited a paired Mg/Ca, $\delta^{18}\text{O}$ analysis. Basin 4, an upper slope mini basin in the northern GoM, is ideally situated (Figures 1.1 and 1.2) for capturing the meltwater routing in the GoM, as it is 200 km west of the location of the paleo-Mississippi River delta of Suter and Berryhill (1985) during MIS 6 and TII. Close proximity to the sediment source led to very high sedimentation rates, as described further in this study, exceeding 6m/ka along the GoM upper slopes of the western shelf of Louisiana and southeastern shelf of Texas, which allows for a high resolution study of MIS6/TII.

Sub-Milankovitch, abrupt climate changes in the $\delta^{18}\text{O}$ records during the MIS 6/TII time interval are analyzed using paired Mg/Ca - $\delta^{18}\text{O}$ measurements to determine if these changes coincide with freshwater routing to the GoM, analogous to cycles observed during MIS 3 (Hill et al., 2006) and the TI (Flower et al., 2004). The phasing of sea surface temperature (SST) and how it relates to changes in $\delta^{18}\text{O}$ of seawater will also be examined.

The timing of a Younger Dryas-like climate reversal observed during TII is studied in relation to changes in the LIS and global sea level using high resolution planktonic foraminifer $\delta^{18}\text{O}$ records as a proxy for higher latitude climate changes. GoM spatial variations in the response to TII meltwater will also be discussed.

1.2 Regional Setting

The Brazos-Trinity drainage system is located within the Texas-Louisiana Slope physiographic province of Martin and Bouma (1978) (Figures 1.1 and 1.2). The slope of the Brazos-Trinity system includes four oval mini basins connected by a system of interbasinal channels first described by Satterfield and Behrens (1990). The shelf in this area contains thick lowstand delta deposits which formed during the late Pleistocene glacial stages (Abdulah et al., 2004; Fraticelli and Anderson, 2003). These deltas are interpreted to be the source for the large volumes of sediment that subsequently infilled the Brazos-Trinity intra-slope basin system (Beaubouef and Friedmann, 2000; Mallarino et al., 2006). Basin 4 is the a mini-basin located at the termination of the Brazos-Trinity drainage system on the upper slope in the northwest GoM in waters ranging from 1000 m at the basin rim to 1500 m at its center (Figure 1.3). No outlets to Basin 4 exist,

indicating that Basin 4 is the final sediment sink for the Brazos-Trinity drainage system, however sediments have partially filled the basin via an abandoned western feeder channel, and an inactive eastern feeder channel that creates the connection to the updip basins. The nature of the sedimentary infill of the four linked mini-basins and its timing in relation to sea level fluctuations (Malarino et al., 2006 and references herein) have been studied in great detail.

However, until the Integrated Ocean Drilling Program (IODP) 2005 Expedition 308, little attention was given to the thick package of muddy sediments blanketing the entire region and underlying the turbidite basin infill sequences within Basin 4. The seismic images of this package show continuous and parallel reflections with slight thickening to the north, indicating that either the source of these deposits lies in a northward direction or at the very least that sedimentation was concentrated in that area. Deposition does not appear affected by the local basin topographic changes (Mallarino et al., 2006) and therefore sedimentation possibly occurred prior to the basin formation itself if it is assumed that topography would affect the sedimentation processes depositing the muddy drape.

1.3 Basin 4 Sediment Sequences

Data used in this study were collected during two different research cruises. IODP Expedition 308, GoM Hydrogeology, was conducted on the D/V JOIDES Resolution in May-July 2005 (Flemings et al., 2006). Two drill sites, 1319A and 1320A, were cored in Basin 4, both of which have been sampled for this study. Hole 1319A is located on Basin 4 southern margin whereas Hole 1320A was drilled in the central part of

the Basin (Figure 1.3; Table 1.1). In addition to the IODP Holes, a Calypso giant piston core MD03-2641 (herein referred to as MD-41) was recovered on the Basin 4 southwestern margin in a very similar setting as, and 3 km northwest of Hole 1319A, as part of the IMAGES program during an earlier (2003) research cruise of the French research vessel *Marion Dufresne* (Figure 1.3: Mallarino et al., 2006).

Hole 1319A and Hole 1320A were drilled and cored to depths of 157.5 m and 299.6 below sea floor (mbsf), respectively. MD-41, a giant piston core, penetrated down to 40 mbsf on Basin 4 slope (Figure 1.3). Slumping and turbidite accumulation disrupt the record starting in the middle of MIS 5 (Mallarino et al., 2006), however there is neither evidence of slumping nor turbidite disruption for the MIS 6/TII interval in the three cores analyzed in this study.

1.4 Methods

Three research groups involved in this study include Rice University in Houston, the Laboratoire des Sciences du Climat et de l'Environnement (LSCE) in Gif sur Yvette, and at Lille University; all were involved in the analyses of Basin 4 sedimentary sequences. The group at Rice University focused on the analyses of IODP Holes 1319A and 1320A, while LSCE and Lille University established the $\delta^{18}\text{O}$ analyses of MD-41 and generously provided the data for this paper.

1.4.1 Stable Isotopes and Mg/Ca

1.4.1.1 Holes 1319A and 1320A

For isotope stratigraphy and Mg/Ca analyses, 80 ~22 cm³ samples were analyzed at a 1.5 m interval in Hole 1320A whereas 262 samples at a 0.75 m interval down Hole

1319A. The samples were disaggregated with Calgon solution and washed over a 63 μm sieve. The $>63 \mu\text{m}$ fraction was dried and dry sieved to retain the $>150 \mu\text{m}$ fraction. From this fraction, 6 to 30 *Globigerinoides ruber* tests (preferably the white variety), a planktonic foraminifer, were picked and washed in an ultrasonic cleaner with distilled water for less than 5 seconds. After being dried, the samples were crushed and mixed, and then split into two subsamples; one for $\delta^{18}\text{O}$ - $\delta^{13}\text{C}$ and the other for Mg/Ca analyses.

The $\delta^{18}\text{O}$ - $\delta^{13}\text{C}$ subsamples were sent to U.C. Davis for $\delta^{18}\text{O}$ and $\delta^{13}\text{C}$ isotopic analyses. For stable isotope $\delta^{18}\text{O}$ and $\delta^{13}\text{C}$ analyses, specimens were ultrasonically cleaned in distilled water after being carefully crushed to release potential sediment infilling. Samples were then heated under vacuum at 375°C for 1/2 hr to remove organic contaminants. Using a common 100% phosphoric acid bath at 90°C , 20-50 micrograms of sample were reacted and analyzed using a GV Instruments Optima isotope ratio mass spectrometer at University of California, Davis. Isotope values are reported in delta notation relative to VPDB. Repeated analyses of a marble working standard (calibrated against the international standard NBS-19) indicate an accuracy and precision of 0.05 ‰ (1σ).

The Mg/Ca subsamples were performed at the Laboratoire des Sciences du Climat et de l'Environnement, Gif sur Yvette. For the Mg/Ca analyses, samples were carefully cleaned following Barker(2003). His method involves an initial sonication to remove fine clays, oxidation of organic matter with a buffered peroxide solution, and a dilute acid leach that eliminates any adsorbed contaminants. Samples were dissolved in weak HNO_3 to yield calcium concentrations of ~ 20 ppm to minimize calcium concentration effects. Foraminiferal Mg and Ca were analyzed on a Varian-VistaPro inductively coupled

plasma – atomic emission spectrometer (ICP-AES) with a cyclonic mini-room and an very low flow atomizer (200 μ l/min). Precision is better than 0.6% on ratios between 1 and 5 mmol/mol.

1.4.2 Ash Layer and *Menardii* Complex

The presence or absence of the planktonic foraminifers *G. menardii* was noted for each sample. Trends in abundances were compared to known and dated patterns for the GoM late Quaternary (Kennett and Huddleston, 1972; Mallarino et al., 2006). One clear ash layer was identified in each Hole, and this ash layer was used, as in Mallarino et al.'s (2006) previous Basin 4 study, to anchor the sedimentary sequence and aid in the correlation between Basin 4 three individual sedimentary sections included in this study

1.4.3 Mg/Ca Derived SST and $\delta^{18}O_{\text{seawater}}$ Calculations

From the Mg/Ca analyzed in *G. ruber* planktonic foraminifers, sea surface temperature (SST) is calculated using a relationship obtained by core top calibration in cores from the tropical Atlantic, and proven valid for the GoM in Flower et al.(2004); $\text{Mg/Ca} = 0.38 \exp(0.090 \text{ SST})$ where Mg/Ca is in mmol/mol and SST is in $^{\circ}\text{C}$ (Dekens et al., 2002). The pooled standard deviation of 70% replicate Mg/Ca analyses is $\pm 2.5\%$ or $\sim 0.3^{\circ}\text{C}$. To subtract out the temperature effect from $\delta^{18}\text{O}$, the equation $T = 14.9 - 4.8 (\delta^{18}\text{O}_c - \delta^{18}\text{O}_{\text{sw}})$, is used; where T is SST in $^{\circ}\text{C}$, the c subscript indicates carbonate, and the sw subscript indicates seawater (from Thunell et al., 1999). Solving the equation for $\delta^{18}\text{O}_{\text{sw}}$ and adding 0.27‰ to convert to the Vienna Standard Mean Ocean Water (VSMOW) standard gives $\delta^{18}\text{O}_{\text{sw}}$ (VSMOW). Total error in this sequence of calculations

is $\pm 3.1\%$. This sequence of calculations follows the procedure set in Flower et al. (2004) and Hill et al. (2006).

1.4.4 Discussion of $\delta^{18}\text{O}$

In stable isotope geochemistry, differences in the isotopic ratios of two samples are generally small and hard to visualize. The δ notation is commonly used to aid in showing these small differences. In this paper, the oxygen isotopic ratio from foraminiferal samples is compared to the ratio from a standard by the expression

(Krauskopf and Bird, 1995):

$$\delta^{18}\text{O}_{\text{foram}} = \left\{ \left[\left(\frac{^{18}\text{O}}{^{16}\text{O}} \right)_{\text{foram}} - \left(\frac{^{18}\text{O}}{^{16}\text{O}} \right)_{\text{standard}} \right] / \left(\frac{^{18}\text{O}}{^{16}\text{O}} \right)_{\text{standard}} \right\} \times 1000\text{‰}$$

Where a $\delta^{18}\text{O}_{\text{foram}}$ positive value indicates enrichment of the sample in ^{18}O relative the standard and a negative value indicates depletion.

Changes in the $\delta^{18}\text{O}$ of seawater is driven by fractionation due to water evaporation and precipitation at ocean surface and in the atmosphere, accumulation and loss of ice at high latitude regions, the mixing of waters with different $\delta^{18}\text{O}$ values such as meltwater and river runoff, as well as the isotopic content of the oceans (Craig and Gordon, 1965; Broecker, 1982). When looking at the changes in $\delta^{18}\text{O}_{\text{foram}}$ values through time, it is assumed that those values reflect the changes in the $\delta^{18}\text{O}$ values of the seawater in which the foraminifers were living. Experiments have shown this relationship to hold true, with a few caveats (Erez and Luz, 1983). Several factors create conditions where the $\delta^{18}\text{O}_{\text{foram}}$ is not in equilibrium with seawater values. These factors include temperature, salinity, vital effects, and the isotopic composition of the water in the location in which the foraminifers are living (Bickert, 2000). Because fresh water can have $\delta^{18}\text{O}$ values as

low as about -60‰ (VSMOW), freshwater can become a major influence on the $\delta^{18}\text{O}$ values recorder in the foraminifer calcite, obviously in relation with the amount of freshwater mixed with the ocean surface waters (Millero, 1996).

Because Basin 4 is located adjacent to the mouth of the paleo-Mississippi (Fig. 1.2), and therefore the potential effects of fresh water input on the $\delta^{18}\text{O}$ values in planktonic foraminifers can become significant, a $\delta^{18}\text{O}$ curve alone is not sufficient for analyzing the paleo-climatologic conditions for the time period of interest in this study. We used, therefore, a second geochemical relationship, Mg/Ca, to attempt to subtract out factors creating disequilibrium between seawater and planktonic foraminifers.

1.4.5 Discussion of Mg/Ca Method

Mg/Ca has been recognized to be a good paleotemperature proxy; once the paleotemperature proxy is combined with $\delta^{18}\text{O}$ analyses in paired samples, the $\delta^{18}\text{O}$ of sea water can be calculated subtracting the temperature effect on the $\delta^{18}\text{O}$ measured in the foraminifer calcite (Lea et al., 2002, Schmidt et al., 2004). When using Mg/Ca paleothermometry to Pleistocene sample material, the possible changes in Mg/Ca of seawater must be considered. Because the residence time of Mg in seawater is ~13 million years (Broecker and Peng, 1982), while the residence time of Ca is ~1 million years (Chester, 2000), the paleo-sea surface temperature records were not affected by a change in Mg/Ca of seawater on shorter timescales. Local Mg and Ca concentrations can be affected by several factors including carbonate deposition (Wilkinson and Algeo, 1989), varying continental weathering rates (Berner et al., 1983), and hydrothermal alteration of basalt at mid-ocean ridges (Elderfield and Schultz, 1996). Because the

timescale on which this study is focused is much smaller than the residence times of both Mg and Ca, and because the local effects on these concentrations is assumed to be minimal, we consider changes to Mg/Ca to be negligible to the data in this study.

1.5 Biostratigraphy and Time Makers

Determining the age-depth profiles for the sediment underlying the turbidites-rich infill in the three Basin 4 sedimentary sections, too old for ^{14}C dating, is possible using several distinct markers. A distinctive ash layer found in all three studied sections is used as first marker to correlate the three sediment sections relative to one another (Figure 1.4a). On the basis of the *Emiliana huxleyii* Acme Zone, the ash layer is identified as the Chocoyos Y8 Ash (Flemings et al., 2006) and dated at 84 ka by Drexler (1980). The second marker is based upon the abundances of *G. menardii*, a species of foraminifers that live in warm tropical waters. Within the Atlantic Ocean, *G. menardii* often disappear during late Pleistocene glacial stages, and re-appears during interglacial stages (Ericson and Wollin, 1956). Zone X represents most of MIS 5 and is observed in the interval just below the 84 ka-old ash layer. Late MIS 6 is a glacial stage during which *G. menardii* tests are known to be completely absent in a sub-zone W1, that lasted only 21 ky, and occurred from 150 to 129 ka according to Kennett and Huddlestun (1972). Figure C.3 shown in the Appendix illustrates background information on terms used throughout this paper to describe the different time subdivisions and the comparisons between these different time intervals. Based on the *G. menardii* sub zonation (Kennett and Huddlestun, 1972), W1 (150-129 ka) is represented in Holes 1319 and 1320A by two sediment intervals at least 127 m and 150 m thick, respectively, corresponding to a time

span not exceeding 21 ky, with the base of both sections being not older than 150 ka. Because *G. menardii* is totally absent in the bottom 6 meters of MD-41, this interval corresponds to at least part of the MIS-6 W1 sub-Zone. The W1 subzone upperboundary is identified at 33.5 mbsf in MD-41 where Zone X begins .

Previous work conducted on Basin 4 established an isotope stratigraphic framework for the turbidite-rich sediment units and extended further down the cores only a few meters below the Y8 ash layer (Mallarino et al., 2006). Because this study looks at the isotope record from the ash layer downward, it becomes an excellent complement to the Mallarino et al. (2006) Basin 4 study.

The three Basin 4 $\delta^{18}\text{O}$ records were plotted with respect to depth (mbsf) due to the age uncertainties associated with MIS 6 and TII (Figure 1.4a). The three records were then hung at each three sites on the W1/X menardi zonation boundary, corresponding to an age of 129 ka, to visually aid the presentation of and the correlation between the three $\delta^{18}\text{O}$ records (Figure 1.4b). Because of the total absence of *G. menardii* at the base of Basin 4 three records, *G. menardii* zonation indicates that only the W1 zone is present and the MIS 6/TII records span no greater than 21 ky (Kennett and Huddlestun, 1972). In addition to the *G. menardii* W1/X zone boundary, the Y8 tephra layer clearly identified at the three sites is also an excellent marker to correlate the three $\delta^{18}\text{O}$ records (Figure 1.4b). Between the two definite markers, the three different $\delta^{18}\text{O}$ records were correlated using the best visual match, by aligning the records next to each other and correlating $\delta^{18}\text{O}$ peaks of similar amplitude and value of millennial-scale $\delta^{18}\text{O}$ oscillations.

1.6 Basin 4 $\delta^{18}\text{O}$ Records

In this study, three $\delta^{18}\text{O}$ curves were produced in Holes 1319A and 1320A, and in core MD03-2641 at least for the sediments immediately underlying the Y8 ash layer (Figures 1.4a and 1.4b).

1.6.1 Hole 1319A

The 1319A $\delta^{18}\text{O}$ record displays at 26.5 and 31.5 mbsf two unusually light values of -3.4‰ and -3.79‰ (VPDB), respectively (Fig. 1.4a). Moreover, the $\delta^{18}\text{O}$ record shows a TII climate reversal from 34 to ~ 32 mbsf (Figure 1.5). Although more apparent in MD-41, values in 1319A reverse themselves from -2‰ at 35 mbsf to close to 0‰ at 34 mbsf. The reversal interval ends with a rapid decrease of the $\delta^{18}\text{O}$ values, reaching a minimum of -3.5‰ slightly below the X/W1 *G. menardii* boundary at 31.6 mbsf. Below this, $\delta^{18}\text{O}$ values quickly become heavier, trending towards 0‰ . Overall, TII spans from 36 to 31 mbsf and has an amplitude of $\sim 3\text{‰}$.

From 35 to 155 mbsf, the $\delta^{18}\text{O}$ record exhibits a series of rapid high amplitude oscillations between 0 and -3‰ . Because of these rapid high amplitude oscillations, the interpretation of the $\delta^{18}\text{O}$ 1319A record during MIS 6/W1 interval was made easier in using a 5-point moving average, plotted over the original data in Figure 1.6. Although the 5-point average curve mutes the rapid and high amplitude $\delta^{18}\text{O}$ oscillations observed during MIS 6/W1, 5 longer term oscillation events, labeled E1-E5 from the youngest to the oldest, can now be identified. These oscillation events have thicknesses ranging from 15 to 30 m. Each event consists first of a series of rapid high amplitude oscillations followed by a sequence of heavier and lower amplitude values.

1.6.2 MD03-2641

Below the Y8 Ash layer, 10 m of section was recovered in MD-41. The $\delta^{18}\text{O}$ record in this interval shows many of the same characteristics as the ones observed in Hole 1319A, but in much higher resolution. However the bottom 10 m of MD-41 represents only the very end of MIS 6/W1 subzone, the complete TII, and most of MIS-5 (Figure 1.7). The two -3.8 and -3.3‰ lightest $\delta^{18}\text{O}$ values in MD-41, at 32.5 and 33.5 mbsf, respectively, agree with the corresponding two lightest $\delta^{18}\text{O}$ values observed in Hole 1319A, with less than 0.3‰ difference in values between the two MD-41 and 1319A records (Figure 1.5). The *G. menardii* X/W1 zone boundary correlation between the two records further demonstrates that these two $\delta^{18}\text{O}$ minima are equivalent in time. A third $\delta^{18}\text{O}$ light value of -3.3‰ observed in MD-41 at 36 mbsf, apparently is not appearing in 1319A most likely due to the greater resolution of the MD-41 record.

The TII climatic reversal interval observed in this record spans from 36 to 33.5 mbsf, with $\delta^{18}\text{O}$ values ranging from <-3‰ at 36 mbsf, falling to ~-1‰ at 34 mbsf. Overall, TII spans from 37.5 to 32.5 mbsf with an overall amplitude of ~3.2‰. The amplitude of the rapid climatic reversal reaches ~2.25‰, while in comparison the 3.75‰ amplitude for the entire deglaciation is quite larger. The thickness and amplitude of the climate reversal observed in MD-41 are very similar to the values seen in 1319A. The very end of the MIS 6/W1 sub-zone is recorded at the bottom of MD-41, with values near 0‰ from 39 to 37.5 mbsf.

The MD-41 $\delta^{18}\text{O}$ record above the ash layer is important to this study because it enables to compare more recent events to those of the MIS 6/W1/TII interval. This

includes the MIS 3 climate oscillations from 21 to 14 mbsf, and the TI meltwater spike at 4 mbsf (Figure 1.7).

1.6.3 1320A

The $\delta^{18}\text{O}$ record for Hole 1320A, used as a complement to the other two high resolution records, displays only one very light -3.2‰ value at 157 mbsf. Because the lack, or paucity of foraminifers from 183 to 157 mbsf in Hole 1320A, $\delta^{18}\text{O}$ analyses could not be generated in this particular interval. From 298 to 183 mbsf, Hole 1320A shows a series of rapid $\delta^{18}\text{O}$ oscillations much like those observed in Hole 1319A in terms of their overall amplitudes of up to $\sim 2.5\text{‰}$, although the resolution of Hole 1320A $\delta^{18}\text{O}$ record is much lower. The 1320A record displays $\delta^{18}\text{O}$ values, 0.4‰ and 0.8‰ at 290 and 268 mbsf, respectively,, that are heavier than any of the values observed in the 1319A record. (Figure 1.4b).

Although Hole 1320A $\delta^{18}\text{O}$ record lacks resolution, this record is important to show that the lightest -3.2‰ value is similar to the two minima observed in the other two 1319A and MD-41 records. Moreover, the overall $\sim 2.5\text{‰}$ amplitudes, for individual events, during the late MIS 6/W1 interval are identical in both Holes 1319A and 1320A.

1.7 Mg/Ca and Related Records

1319A was sampled at 73 individual core levels between 96 and 27 mbsf (an average spacing of 75 cm, except where a lack of foraminifers prohibited the dual analyses) and were split into two aliquots for paired $\delta^{18}\text{O}$ ($\sim 0.1\text{mg}$) (Figure 1.8a) – Mg/Ca ($\sim 0.3\text{mg}$) (Figure 1.8b) analyses. The paired analyses of these samples cover the

upper half of E3, all of E2 and E1, up through TII and MIS 5.5 (Figure 1.6). Mg/Ca ratios range between 3.0 and 5.8 (mmol/mol), with a trend of decreasing values from E3 through E1, while the onset of TII marks a rapid increase in values. Because temperatures are directly derived from the Mg/Ca ratios, the trends in the temperature curve (Figure 1.8c) obviously mimic the Mg/Ca curve, with overall SST temperatures ranging from 22.7 to 30.3°C. A general cooling trend from E3 to E1, from 29.5°C to 23.8°C, and then a rapid warming, rising from 23.8°C to 30.3°C during TII are observed. Fairly constant and average temperature values (26.5 to 28 °C) are displayed within the first half of MIS 5.

$\delta^{18}\text{O}_{\text{sw}}$ (Figure 1.8d) reflects sea water oxygen isotopic composition after the temperature effect has been subtracted out. Isolating the data in this way, the excursion during the E3 event increases to ~2.2‰, a new event exceeding 1.2‰ appears during E2, and while the overall amplitude of the E1 sequence remains about the same at 1.9‰, the events become more orderly, with a trend of decreasing amplitude with time. The $\delta^{18}\text{O}_{\text{sw}}$ range during TII displays a total amplitude of 2‰ and is one of the three largest amplitude events in the 1319A record. A lack of data points during the TII climate reversal prohibits the analysis of this event using the paired data. The end of TII marks an equally dramatic drop of 1.8‰, and represents the end of MIS 5.5 and a transition into MIS 5.4. The last rise in values of 1.5‰ corresponds to the transition from MIS 5.4 to MIS 5.3.

1.8 Discussion

In this study, TII and MIS 6/W1 millennial-scale climate oscillations have been described for Basin 4. The TII meltwater pulse and MIS 6/W1 climate oscillations display close similarities to rapid climate changes observed in the GoM (in particular the Orca Basin) during younger and better constrained by absolute dating TI and MIS 3 time intervals. (Flower et al., 2004; Hill et al., 2006). analysis and comparison of the Basin 4 record. The Red Sea record (Siddall et al., 2007) of the TII climatic reversal provides a chronology for the event, and the Basin 4 record links the changes in sea level observed in the Red Sea to meltwater pulses of the LIS.

1.8.1 Termination II Meltwater Pulse

During Termination I, the transition from Last Glacial Maximum (LGM) to the current interglacial MIS 1, or Holocene, large volumes of glacial meltwater were flushed into the Gulf of Mexico via the paleo-Mississippi River in rapid and distinct pulses that appear as isotopically light values in the planktonic foraminiferal $\delta^{18}\text{O}$ record (Kennett and Shackleton, 1975; Aharon, 2003 and references therein). The influence of this isotopically light melt water derived from the North American Ice Sheet on the Gulf of Mexico surface water $\delta^{18}\text{O}$ record is especially well established in the Orca Basin for the last deglaciation (Shackleton and Opdyke, 1973; Flower and Kennett, 1990; Flower et al., 2004) and can be seen as a -4‰ sharp minimum in the Basin 4 record of MD-41 (Figures 1.7 and 1.9). Williams (1982) predicted that the magnitude of the response to pulses of melt water in the Gulf of Mexico had to be a function of distance from the source of the fresh water discharge and the overall prevailing current direction, with a linear decrease

in meltwater response with increasing distance away from the discharge source and a prevailing westward flowing current muting the response eastward of the discharge point during Termination I (Figures 1.2, 1.9). To explain this discrepancy, modern surface ocean currents in the northern GoM are assumed to be similar to currents in the gulf during TI. Discharge from the Mississippi River is carried west by currents (Smith, 1980) and mixed with the isotopically heavier gulf waters. By the time the discharge water is carried to the eastern side of the gulf, the isotopic signature of the meltwater is muted due to the mixing effect (Figure 1.9; Williams, 1984).

The Termination I meltwater response for Basin 4, using the Williams (1984) data, would predict $\delta^{18}\text{O}$ values which should not exceed $\sim 2.5\text{‰}$ and stipulates that values for any point in the Gulf of Mexico should not exceed -4.0‰ . The actual response in Basin 4 however is much greater than the predicted value, reaching -4.0‰ in cores MD-41 (this study), MD03-2642, and MD03-2633, and the largest value in core MD03-2637 at -6.0‰ (Mallarino et al., 2006; Figure 1.3). Because these values greatly exceed the predicted response, currents must obviously play a more important role in focusing the meltwater signal than was previously suggested (Figures 1.2 and 1.9).

Termination II also displays a meltwater response in the GoM $\delta^{18}\text{O}$ planktonic foraminiferal records (Figure 1.9). Three records show a similar response, with values around -2.0‰ (Falls, 1980; Tripsanas et al., 2007; Joyce et al., 1990). Basin 4 $\delta^{18}\text{O}$ values for the same TII meltwater event are much lighter than these studies, the data from Hole 1319A and MD-41 agree closely with each other, at -3.5‰ to -3.79‰ respectively (Figure 1.4b). This is especially surprising given the location of the Bryant Canyon core JPC 31 (Figures 1.2 and 1.9), less than ~ 200 km SSE from the mouth of the paleo-

Mississippi river (Tripanas et al., 2007), nearly the same distance to Basin 4; ESE at ~200 km. Westward trending surface currents, observed in this part of the modern GoM and thought to have occurred during Termination I (Williams, 1984), must have also existed during Termination II. The plume of isotopically light $\delta^{18}\text{O}$ meltwater was most likely pushed westward, across the Basin 4 area before mixing with the gulf waters. Only a very small plume of isotopically light meltwater, relatively isolated from the main freshwater plume by the westward currents, had to reach the Bryant Canyon area to explain the muted signal in core JPC 31 (Figures 1.2 and 1.9). These observations also agree with circulation patterns established in the modeling of Gulf of Mexico currents during the last glacial period (Brunner and Cooley, 1976). Alternatively, though not likely, the muted response in the Bryant Canyon cores could be at least partially explained by the observed lower sedimentation rates in core JPC 31 relative to the high sedimentation rates observed in the Basin 4 sediment accumulation. Relatively light $\delta^{18}\text{O}$ values in the surface of the GoM at the location of core JPC 31, would be averaged (muted) over a greater time span than the in the Basin 4 cores. This averaging effect can occur where sedimentation rates are low enough that one of these events is either much thinner than the 0.5 cm sample thickness used in this study or/and effect of bioturbation is enhanced by the low sedimentation rates.

In Basin 4, Mg/Ca derived SST at the beginning of TII in 1319A is ~25°C before the meltwater pulse itself; the temperatures quickly rise during the pulse to more than 30°C, followed by a perceived precipitous fall (which is due to the condensed section of hemipelagic sediment that begins at ~32 mbsf and marks a rapidly reduced sedimentation rate when compared to the clay sediments below it), and leveling off at ~27.5°C after the

meltwater pulse episode. In the Orca Basin, SSTs for TI are $\sim 24^{\circ}\text{C}$ before the meltwater pulse, and rise to $\sim 28 - 29^{\circ}\text{C}$ during and after the meltwater pulse episode (Flower, 2004). Therefore, the two records show similar character and values (Figure 1.10a) with temperatures increasing a total of 4°C during TI in the Orca Basin and $\sim 5^{\circ}\text{C}$ during TII in Basin 4. $\delta^{18}\text{O}_{\text{sw}}$ meltwater values for TII show a total amplitude of 2‰ as compared to the $\sim 3\text{‰}$ amplitude of TI (Figure 1.10b). While TII is more muted than TI, much of this difference might have to do with the resolution in 1319A. MD-41 has a $\delta^{18}\text{O}$ amplitude of $\sim 4\text{‰}$, the lower resolution 1319A record used for the paired $\delta^{18}\text{O} - \text{Mg/Ca}$ only has an amplitude of $\sim 3\text{‰}$. It is therefore possible that higher resolution sampling, planned in a follow up study, would yield similar amplitudes as seen in the high resolution, $\delta^{18}\text{O}_{\text{sw}}$ Orca Basin record. Because the 1319A and MD-41 TII $\delta^{18}\text{O}$ meltwater values are similar to meltwater $\delta^{18}\text{O}$ minimum values for TI in MD-41 (minimum values near -4‰) (Figure 1.7), and the TII SST and $\delta^{18}\text{O}_{\text{sw}}$ curves for 1319A are comparable to those from TI in the Orca Basin (Figure 1.10), we conclude that similar millennial-time scale climate oscillations affecting the GoM during TI were also occurring during TII, and can be explained as pulses of isotopically light LIS meltwater (Flower et al., 2004).

1.8.2 Termination II Reversal

Various records, both terrestrial and oceanic, show that a Younger Dryas-like climate reversal occurred during Termination II (Seidenkrantz et al., 1996; Cannariato and Kennett, 2005; Siddall et al., 2007 and references therein). This climate reversal is recognized as being global, with records from the previous references showing a significant, correlatable cooling event in the northern hemisphere. Quantifying the

duration and magnitude of the reversal is difficult, and each study conducted on this time period has weaknesses such as discontinuous records, lack of dating or dating with significant error bars. Speleothem hiatuses in Norway date the duration of this event from $132 \text{ ka} \pm 6.0 \text{ ka}$ to $128 \text{ ka} \pm 8.8 \text{ ka}$ (Lauritzen, 1995). These dates largely agree with other studies which show the end of an early Termination II highstand, using U/Th dates on Barbados corals, beginning after 133.5 ka (Thompson and Goldstein, 2005) and the end of a Termination II sea level fall, using U/Th dating on Aladdin's Cave corals, to occur at 126 ka - 134 ka (Stirling et al., 1998) or an average of 130 ka (Siddall et al., 2007).

The magnitude of sea level fall during the TII climate reversal has been estimated at 55 to 75 m in relative sea level change using Huon Peninsula corals (Esat et al., 1999), and between $30 \text{ m} \pm 12 \text{ m}$ and $40 \pm 12 \text{ m}$ in relative sea level change in the Red Sea using $\delta^{18}\text{O}$ of *G. ruber* (Siddall et al., 2007). The error in these estimates is potentially significant due to the tectonic activity and uncertainty in uplift rates of the Huon Peninsula, and the fact that the Red Sea method has previously been shown to underestimate sea level changes during Termination I (Antonioli et al., 2004). While understanding this uncertainty, we bracket the actual sea level fall between 30 and 75 m for this event using the smallest and largest values from these studies as our upper and lower bounds to bracket the magnitude of sea level change during this time.

The cooling during Termination II created a two-step deglaciation during the glacial MIS-6 to interglacial MIS-5 transition and demonstrates that the Younger Dryas cooling interval was not a unique phenomenon (Seidenkrantz et al., 1996). However, these two events do not have a direct one-to-one correlation. Termination I records are

punctuated by a series of three very rapid, meltwater pulse-derived sea level rises (Alley et al., 2005) and countering cooling events, however there is no evidence for events with measurable sea level falls (Fairbanks, 1989; Bard et al., 1990). This contrasts to the tens of meters of sea level fall believed to be associated with the Termination II reversal (Siddall et al., 2007).

$\delta^{18}\text{O}$ records from MD-41 and Hole 1319A clearly show the Termination II climate reversal (Figure 1.5). While many studies have noted the existence of this event, it has never before been described in a GoM climate record. The Basin 4 records reinforce the argument that a significant worldwide cooling event occurred in marginal basins such as in the Santa Barbara Basin (Cannariato and Kennett, 2005), open oceans (Seidenkrantz et al., 1996), and on the continents (Schweger and Matthews, 1991) during this time by adding the GoM to the list of locations where this cooling event has occurred.

The beginning and end of the Termination II cold reversal in the MD-41 records is marked by meltwater pulses with $\delta^{18}\text{O}$ values of -3.25‰ and -3.15‰, which is much lighter than the other points in the MIS 6/Termination II record in Basin 4. The very end of Termination II is marked by the largest meltwater pulse, recording values up to -3.8‰ in MD-41 (Figure 1.5).

The cold reversal is bracketed between two large meltwater pulses into the Gulf of Mexico, which is a contrast to the Younger Dryas, an event that came after the major Termination I meltwater pulse events into the Gulf of Mexico had ended, with Laurentide Ice Sheet meltwater subsequently redirected into the North Atlantic (Marchitto and Wei, 1995). The cause of the Younger Dryas is thought to be linked to the eastward routing of

the Laurentide meltwater and shutdown of the North Atlantic deep water formation (Berger, 1990; Muscheler et al., 2000). If this series of events is also the cause for the Termination II cold reversal, the Basin 4 record of the reversal between two large meltwater pulses (Figure 1.5) provides an important chronology to the deglaciation and implies an early routing of meltwater to the North Atlantic and Gulf of Mexico, followed by cooling with associated sea level drop and ice sheet buildup, abruptly ending with a second large flux of meltwater into the Gulf of Mexico.

1.8.3 MIS 6/W-1 Interstadial

Greenland ice cores archive dramatic and abrupt climatic changes at millennial to decadal time scales during the last 80 ka in the northern hemisphere (Alley et al., 2000). Abrupt climate changes observed during MIS 6/W-1 are similar in character and duration to the MIS 3 oscillations, and are found globally (Cannariato and Kennett, 2005). Basin 4 records include an expanded interval preceding TII (Figure 1.4b), with oscillations similar to the MIS 6 interstadials of the Santa Barbara Basin (Kennett et al., 2000) and the MIS 3 climate oscillations in the Orca Basin (Hill et al, 2006). We use the higher resolution record in 1319A for discussion; however, 1320A confirms that high amplitude oscillations do exist in Basin 4.

Sea level was ~ 80 to 120 m below present during MIS 6/W1 (Chappell, 2002; Shackleton, 2000; Martinson et al., 1987; Imbrie et al., 1984; with $\delta^{18}\text{O}$ records converted to sea level in Bard et al., 2002) expected $\delta^{18}\text{O}$ enrichment values are from ~ 0.7 to 1.0‰ based on the relationship 0.083‰ per 10m sea level change (Adkins and Schrag, 2001). Values $\leq -1.6\text{‰}$ would indicate that sea surface temperatures were more than 3°C higher

than the average modern Gulf of Mexico summer temperatures of 29 °C (Levitus, 2005), which is prohibitively large to explain such $\delta^{18}\text{O}$ anomalies (Flower, 2004) (using the equation $T = 14.9 - 4.8 [\delta^{18}\text{O}_c - \delta^{18}\text{O}_{sw}]$ where T is in degrees centigrade, the subscript c indicates carbonate, and the subscript sw indicates seawater; Thunell et al., 1999).

SSTs from Mg/Ca measurements verify that maximum temperature during MIS 6/W1 was a maximum of 28.8 °C and a minimum of 23.5 °C during MIS 6/W1 (Figure 1.8c). This is, as expected, relatively colder than the today's mean of 29 °C (Levitus, 2005), but is in agreement with temperature variations observed in Orca Basin climate oscillations during MIS 3 (Figure 1.11a). $\delta^{18}\text{O}_{sw}$ values for MIS 6/M1 in Basin 4 also fall within the range of those calculated in the Orca Basin during MIS 3 (Figure 1.11b). MD-41 has a detailed history of MIS 3 (Figure 1.7) and when compared to the MIS 6/W1 record in 1319A, there are striking similarities (Figure 1.12). MIS 6/W1 $\delta^{18}\text{O}$ values are slightly heavier than the MIS 3 $\delta^{18}\text{O}$ values, which can be attributed to the end of MIS 6 being a fully glacial interval, whereas the MIS 3 is an interstadial, and has interstadial $\delta^{18}\text{O}$ values. The Orca Basin record during MIS 3 has shown how isotopically light Laurentide Ice Sheet meltwater affected the GoM planktonic foraminifer $\delta^{18}\text{O}$ values. These MIS 3 meltwater events in the Orca Basin do not correlate to D/O cycles seen in the Greenland air temperature record, but rather to Antarctic warming events (Hill et al., 2006) as this conclusion had been already to be the case for TI (Flower et al., 2004).

Because the amplitudes and character of the events seen in Basin 4 are similar to those in MD-41 during MIS 3, and also Orca Basin MIS 3 melting events as seen in the SST and $\delta^{18}\text{O}_{sw}$ records, the Basin 4 MIS 6 events must be a record of LIS melting during MIS 6. The amplitude of the MIS 6 $\delta^{18}\text{O}_{sw}$ events is largely a response to the meltwater

draining from the paleo-Mississippi river and pushed by surface currents into the area of Basin 4.

Chronology can be estimated for the record using the analogs previously discussed. MIS 3 events lasted anywhere from 2-4 ka in the Orca Basin (Hill et al., 2006), while MIS 6 events in the Santa Barbara Basin (Cannariato and Kennett, 2005) lasted from 2.5-4 ka, depending on different chronologies. Applying this to our record, the bottom 120 m of the 1319A core represents approximately 13 - 20 ka of MIS 6. This largely agrees with the age constraints using *G. menardii* zonation, which bracketed the MIS 6 record at no longer than 21 ka. The age of the oldest part of 1319A lies between 148 and 156 ka using these constraints. These age constraints allow us to calculate sedimentation rates in Basin 4 during MIS 6, which were fairly rapid; on the order of ~ 6 to 9 m per thousand years.

1.9 Conclusions

The greatly expanded record of Basin 4 has provided a detailed history of TII/Late MIS 6 using $\delta^{18}\text{O}$ of planktonic foraminifer *G. ruber* (white variety) with paired Mg/Ca measurements. In the $\delta^{18}\text{O}$ record, a series of millennial-scale climate oscillations are identified throughout MIS 6. Also, rapid climate oscillations during TII show a climate reversal with a $\delta^{18}\text{O}$ amplitude greater than 1.2‰, and several meltwater spikes approaching values of -4‰. Paired $\delta^{18}\text{O}$ – Mg/Ca measurements are used to estimate variations in SST. These SST values are used to correct $\delta^{18}\text{O}$ for SST variabilities and derive $\delta^{18}\text{O}_{\text{sw}}$, which gives information on the meltwater events entering the northern Gulf of Mexico.

SST based on Mg/Ca ratios show an overall cooling trend through the end of MIS 6, reaching $\sim 24^{\circ}\text{C}$ at its coolest. Temperatures during TII quickly increased, reaching a peak values at $\sim 29 - 30^{\circ}\text{C}$. The $\delta^{18}\text{O}_{\text{sw}}$ record shows several features that were not clear in the $\delta^{18}\text{O}$ curve, including higher amplitudes during MIS 6 event E3, a second peak in E2, and a tapering of events during E1. In the $\delta^{18}\text{O}_{\text{sw}}$ record during TII, meltwater pulse amplitude decreases to 2‰ due to the large temperature increase during this time, however only $\sim 1\%$ of this amplitude can be explained by the increase in sea level. The $\delta^{18}\text{O}$ MIS 6/TII record in Basin 4 is intimately linked to millennial-scale events, namely meltwater pulses, originating from the LIS and routed into the northern Gulf of Mexico through the paleo-Mississippi river.

These results confirm other study's descriptions of MIS 6/TII millennial-scale climate oscillations (Cannariato and Kennett, 2005) and link them to changes in the LIS via meltwater routing into the GoM. $\delta^{18}\text{O}$, SST, and $\delta^{18}\text{O}_{\text{sw}}$ records during MIS 3/ TI (Flower et al., 2004; Hill et al., 2006) are comparable to the results found in this study and we hypothesize that the sub-Milankovitch forcing mechanisms at work during MIS 3/ TI also explain the Basin 4 record of MIS 6/TII, although this is nearly impossible to ascertain without a northern hemisphere ice sheet record. Because a northern hemisphere ice record older than MIS 5 does not exist, we conclude that the Basin 4 MIS 6/TII record could be used as a proxy for the growth and decay cycles of the LIS via the timing of meltwater events seen in the planktonic foraminiferal $\delta^{18}\text{O}$ values.

REFERENCES

- Abdulah, K.C, Anderson, J.B., Snow, J.B., and. Holdford-Jack, L, 2004, The Late Quaternary Brazos and Colorado Deltas, Offshore Texas: Their Evolution and the Factors That Controlled Their Deposition." *Special Publication, Society of Sedimentary Research*, 79, p. 237-270.
- Adkins, J. R., and D. P. Schrag, 2001, Pore fluid constraints on deep ocean temperature and salinity during the last glacial maximum, *Geophys. Res. Lett.*, 28, 771–774.
- Aharon, P., 2003, Meltwater flooding events in the Gulf of Mexico revisited: Implications for rapid climate changes during the last deglaciation, *Paleoceanography*, 18(4), 1079, doi:10.1029/2002PA000840.
- Alley, Richard B; Clark, Peter U, Huybrechts, Philippe, Joughin, Ian, 2005, Ice-sheet and sea-level changes *Science*, v.310, no.5747, p.456-460.
- Alley, Richard B., 2000, Ice core evidence of abrupt climate changes, *Proceedings of the National Academy of Sciences*, Vol. 97, Issue 4, p. 1331-1334.
- Antonioli, F., Bard, E., Potter, E.K., Silenzi, S., and Imbrota, S., 2004, 215-ka history of sea-level oscillations from marine and continental layers in Argentarola Cave speleothems (Italy): *Global and Planetary Change*, v. 43, no. 1–2, p. 57–78, doi: 10.1016/j.gloplacha.2004.02.04.
- Bard, E., Hamelin, B., and Fairbanks, R.G., 1990, U-Th ages obtained by mass-spectrometry in corals from Barbados—Sea level during the past 130,000 years: *Nature*, v. 346, no. 6283, p. 456–458, doi: 10.1038/346456a0.
- Bard, E., Fabrizio Antonioli, Sergio Silenzi, 2002, Sea-level during the penultimate interglacial period based on a submerged stalagmite from Argentarola Cave (Italy), *Earth and Planetary Science Letters*, 196, p. 135-146
- Beaubouef, R.T., and J.T. Friedmann, 2000, High Resolution Seismic/Sequence Stratigraphic Framework for the Evolution of Pleistocene Intra Slope Basins, Western Gulf of Mexico: Depositional Models and Reservoir Analogs, GCSSEPM Foundation 20th Annual Research Conference, Deep Water Reservoirs of the World, Dec. 3-6, 2000.
- Berger, W.H., 1990, The Younger Dryas cold spell – a quest for causes, *Paleogeography, Paleoclimatology, Paleoecology*, 89, p.219-237.
- Berner, R.A., Lasaga, A.C., and Garrels, R.M., 1983, The carbonate-silicate geochemical cycle and its effect on atmospheric carbon dioxide over the past 100 million years. *Am. J. Sci.*, 283:641–683.

Bickert, Torsten, 2000, Influence of Geochemical Processes on Stable Isotope Distribution in Marine Sediments, in *Marine Geochemistry*, edited by Horst D. Schulz and Matthias Zabel, p. 309-333, Springer, New York.

Broecker, W.S., and Peng, T.-H., 1982, *Tracers in the Sea*: Palisades, NY (Eldigio Press).

Broecker, W.S., 1982, Ocean chemistry during glacial time. *Geochimica et Cosmochimica Acta*, 46: 1689-1705.

Brunner, Charlotte A., and Judith F. Cooley, 1976, Circulation in the Gulf of Mexico during the last glacial maximum 18,000 yr ago, *Geological Society of America Bulletin*, v. 87, p. 681-686, doc. no. 60506.

Cannariato, Kevin G., and James P. Kennett, 2005, Structure of the Penultimate Deglaciation along the California Margin and Implications for Milankovitch Theory, *Geology*, 33, no. 2, p. 157-160.

Chappell, J., 2002, Sea level changes forced ice breakouts in the Last Glacial cycle: new results coral terraces. *Quaternary Science Reviews*, 21, p. 1229-1240.

Chappellaz, Jerome, E. Brook, T. Blunier, and B. Malaize, 1997, CH₄ and $\delta^{18}\text{O}$ of O₂ records from the Antarctic and Greenland Ice: A Clue for Stratigraphic Disturbance In the Bottom Part of the Greenland Ice Core Project and the Greenland Ice Sheet Project 2 Ice Cores: *Journal of Geophysical Research*, v. 102, no. C12, p. 26,547 – 26,557.

Chester, Roy, 2000, *Marine Geochemistry—2nd Ed.*, 506 p., Blackwell Science, Malden, MA.

Craig, H., and Gordon, L.I., 1965. Deuterium and oxygen-18 variations in the ocean and marine atmosphere. In: Tongiari, E. (ed.), *Stable isotopes in oceanic studies and paleotemperatures*, Consiglio Nazionale Delle Ricerche, Laboratorio di Geologia Nucleare, Pisa, p. 9-130.

Dansgaard, W., S. J. Johnsen H. B. Clausen D. Dahl-Jensen N. S. Gundestrup C. U. Hammer C. S. Hvidberg J. P. Steffensen A. E. Sveinbjörnsdottir J. Jouzel & G. Bond, 1993, Evidence for general instability of past climate from a 250-kyr ice-core record, *Nature* 364, 218 - 220.

Dekens, P.S., Lea, D.W., Pak, D.K., and Spero, H.J., 2002, Core top calibration of Mg/Ca in tropical foraminifers: Refining paleotemperature estimation: *Geochemistry, Geophysics, Geosystems*, v. 3, doi: 10.129/2001/GC000200.

Drexler, J. W., W. I. Rose, R. S. J. Sparks, and M. T. Ledbetter, 1980, The Los Chocoyos ash, Guatemala: A major stratigraphic marker in Middle America and in three ocean basins: *Quaternary Research*, v. 13, p. 327–345.

Elderfield, H., and Schultz, A., 1996, Mid-ocean ridge hydrothermal fluxes and the chemical composition of the ocean. *Annu. Rev. Earth Planet. Sci.*, 24(1):191–224.

Erez, J. and Luz, B., 1983, Experimental paleotemperature equation for planktonic foraminifera. *Geochimica et Cosmochimica Acta*, 47, p. 1025-1031.

Ericson, D. B., and G. Wollin, 1956, Correlation of six cores from the equatorial Atlantic and the Caribbean: *Deep-Sea Research*, v. 3, p. 104–125.

Esat, T.M., McCulloch, M.T., Chappell, J., Pillans, B., and Omura, A., 1999, Rapid fluctuations in sea level recorded at Huon Peninsula during the penultimate deglaciation: *Science*, v. 283, no. 5399, p. 197–201, doi: 10.1126/science.283.5399.197.

Fairbanks, R.G., 1989, A 17,000-year glacioeustatic sea-level record—Influence of glacial melting rates on the Younger Dryas event and deep ocean circulation: *Nature*, v. 342, no. 6250, p. 637–642, doi: 10.1038/342637a0.

Flemings, P.B., Behrmann, J.H., John, C.M., and the Expedition 308 Scientists, 2006. Proc. IODP, 308: College Station TX (Integrated Ocean Drilling Program Management International, Inc.)

Flower, B.P., and Kennett, J.P., 1990, The Younger Dryas cool episode in the Gulf of Mexico: *Paleoceanography*, v. 5, p. 949–961.

Flower, Benjamin P., David W. Hasings, Heather W. Hill, and Terrence M. Quinn, 2004, Phasing of deglacial warming and Laurentide Ice Sheet meltwater in the Gulf of Mexico, *Geology*, v. 32, no. 7, p. 597–600.

Fratlicelli, C.M, and Anderson, J.B. "The impact of the Brazos deltaic system on upper slope stratigraphic sequence evolution." *Shelf Margin Deltas and Linked Down Slope Petroleum Systems: Global Significance and Future Exploration Potential*, 23 (12/2003): 325-357.

Hays, J.D., Imbrie, J., Shackleton, N.J., 1976, Variations in the Earth's Orbit: Pacemaker of the Ice Ages, *Science*, v.194, no. 4270, p. 1121-1132. doi:10.1126/science.194.4270.1121.

Hill, H. W., B.P. Flower, T.M. Quinn, D.J. Hollander, T. P. Guilderson, 2006, Laurentide Ice Sheet meltwater and abrupt climate change during the last glaciation, *Paleoceanography*, vol. 21, pa1006, doi:10.1029/2005PA001186.

Huber, Markus Leuenbergera, Renato Spahnia, Jacqueline Flückigera, Jakob Schwandera, Thomas F. Stockera, Sigfus Johnsen, Amaelle Landais, and Jean Jouzeld, 2006, Isotope calibrated Greenland temperature record over Marine Isotope Stage 3 and its relation to CH₄. *Earth Planet. Sci. Lett.* 245, p. 504–519.

Imbrie, J., J.D. Hays, D.G. Martinson, A. McIntyre, A.C. Mix, J.J. Morley, N.G. Pisias, W.L. Prell, N.J. Shackleton, 1984, The orbital theory of Pleistocene climate: support from a revised chronology of the marine $\delta^{18}\text{O}$ record, in: A.L. Berger et al. (Eds.), *Milankovitch and Climate, Part 1*, Reidel, p. 269–305.

Johnsen, S.J., and 14 others, 1997, The $\delta^{18}\text{O}$ Record Along the Greenland Ice Core Project Deep Sea Ice Core and the Problem of Possible Eemian Climatic Instability: *Journal of Geophysical Research*, v. 102, no. C12, p. 26,397-26,410.

Kennett, J.P., and P. Huddleston, 1972, Late Pleistocene paleoclimatology, foraminiferal biostratigraphy, and tephrocronology: Western Gulf of Mexico: *Geology*, v. 21, no. 6, p. 483-486.

Kennett, J.P., and Shackleton, N.J., 1975, Laurentide ice sheet meltwater recorded in Gulf of Mexico deep-sea cores, *Science*, 188, p. 147-150.

Kennett, J.P., Cannariato, K.G., Hendy, I.L., and Behl, R.J., 2000, Carbon isotopic evidence for methane hydrate instability during Quaternary interstadials: *Science*, v. 288, p. 128–133.

Krauskopf, Konrad B., and Dennis K. Bird, 1995, *Introduction to Geochemistry--3rd Ed.*, 647p., St. Louis.

Laj, Carlo; Shipboard Scientific Party, 2006, Physical properties of sediment core MD03-2641, doi:10.1594/PANGAEA.465127

Landais, A., N. Caillonia, C. Goujonb, A.M. Grachevc, J.M. Barnolab, J. Chappellazb, J. Jouzela, V. Masson-Delmottea, and M. Leuenberger, 2004, Quantification of rapid temperature change during DO event 12 and phasing with methane inferred from air isotopic measurements, *Earth Planet. Sci. Lett.*, 225, p. 221–232.

Lauritzen, S.E. 1995, High-resolution paleotemperature proxy record during the last interglaciation in Norway from speleothems. *Quaternary Research*, 43,133-146.

Lambeck, Kurt, and John Chappell, 2001, Sea level change through the last glacial cycle, *Science*, v. 292, no. 5517, p. 679-686.

Lea, D.W., Pak, D.K., and Spero, H.J., 2000, Climate impact of late Quaternary equatorial Pacific sea surface temperature variations, *Science*, 289(5485):1719–1724.

Leventer, A., D.F. Williams, and J. P. Kennett, 1982, Dynamics of Laurentide ice sheet during the last glaciation: Evidence from the Gulf of Mexico, *Earth and Planetary Science Letters*, 59, p. 11-17.

- Levitus, S., 2005, National Oceanographic Data Center World Ocean Atlas 1994, http://www.nodc.noaa.gov/OC5/WOA01/1d_woa01.html, Earth Syst. Res., Phys. Sci. Div., Natl. Oceanic and Atmos. Admin., Boulder, Colo.
- Mallarino, G., R. T. Beaubouef, A. W. Droxler, V. Abreu, and L. Labeyrie, 2006, Sea Level influence on the nature and timing of a minibasin sedimentary fill (northwestern slope of the Gulf of Mexico): AAPG Bulletin, v. 90, no. 7, p. 1089-1119.
- Marchitto, T. M., and K.Y. Wei, 1995, History of Laurentide meltwater flow to the Gulf of Mexico during the last deglaciation, as revealed by reworked calcareous nannofossils, *Geology*, 23, 779-782.
- Martin, R.G., and A. Bouma, 1978. Physiography of the Gulf of Mexico, in A. Bouma, G.T. Moore, and J.M. Coleman eds., Framework facies, and oil trapping characteristics of the upper continental margin, AAPG, Studies in Geology 7.
- Martinson, D.G., N.G. Pisias, J.D. Hays, J. Imbrie, T.C. Moore and N.J. Shackleton, 1987, Age dating and the orbital theory of the ice ages: development of a high-resolution 0 to 300,000-year chronostratigraphy. *Quat. Res.* 27, p. 1-29.
- Millero, Frank J., 1996, *Chemical Oceanography—2nd Ed*, 469p., CRC Press, New York.
- Muller, Richard A., and Gordon J. MacDonald, 1997, Glacial Cycles and Astronomical Forcing, *Science* v.277, p. 215-218.
- Muscheler, R., J. Beer, G. Wagner, and R.C. Finkel, 2000, Changes in deep-water formation during the Younger Dryas event inferred from ¹⁰Be and ¹⁴C records, *Nature*, 408, p. 567-570.
- Rasmussen, Tine L., E. Balbon, E. Thomsen, L. Labeyrie, and T.C.E. van Weering, 1999, Climate Records and Changes in Deep Outflow from the Norwegian Sea ~150-55 ka: *Terra Nova*, v. 11, no. 2/3, p. 61-66.
- Satterfield, W.M., and E.W. Behrens, 1990, A Late Quaternary Canyon/Channel System Northwest Gulf of Mexico Continental Slope, *Marine Geology*, 92, p. 51-67.
- Schmidt, M.W., Spero, H.J., and Lea, D.W., 2004, Links between salinity variation in the Caribbean and North Atlantic thermohaline circulation. *Nature*, 428(6979):160-163.
- Schweger, C.E. and Matthews, J.V., 1991, The last interglaciation in the Yukon: comparisons with Holocene and interstadial pollen records. *Quaternary International*, 10-12, 85-94.
- Seidenkrantz, Marit-Solveig, Lennart Bornmalm, Sigfus J. Johnsen, Karen Luise Knudsen, Antoon Kuijpers, Stein-Eric Lauritzen, Suzanne A.G. Leroy, Isabelle Mergeai, Charles Schweger, and Brigitte Van Vliet-Lanoe, 1996, Two-Step Deglaciation at the

Oxygen Isotope Stage 6/5E Transition: The Zeifen-Kattegat Climate Oscillation, *Quaternary Science Reviews*, 15, p. 63-75.

Shackleton, N.J., and M. A. Hall, Oxygen and carbon isotope Stratigraphy of DSDP hole 552A: Plio_Pleistocene glacial history, Initial Rep. Deep Sea Drill. Proj., 81, 599-609, 1984.

Shackleton, N.J., 2000, The 100,000-year ice-age cycle identified and found to lag temperature, carbon dioxide, and orbital eccentricity. *Science* 289, p. 1897-1902.

Siddall, M., E. J. Rohling, A. Almogi-Labin, C. Hemleben, D. Meischner, I. Schmelzer, and D. A. Smeed, 2003, Sea-level fluctuations during the last glacial cycle, *Nature*, v.423, p. 853- 858.

Siddall, Mark, Edouard Bard, Eelco J. Rohling, Christoph Hemlebin, 2007, Sea-level Reversal During Termination II, *Geology*, 34, no. 10, p.817-820.

Smith, N.P., 1980, On the hydrography of shelf waters off the central Texas Gulf coast, *J. Phys. Oceanogr.*, 10, 806-813.

Stirling, C.H., Esat, T.M., Lambeck, K., and Mc-Culloch, M.T., 1998, Timing and duration of the last interglacial: Evidence for a restricted interval of widespread coral reef growth: *Earth and Planetary Science Letters*, v. 160, no. 3-4, p. 745-762, doi: 10.1016/S0012-821X(98)00125-3.

Suter, J.R., and H.L. Berryhill Jr., 1985, Late Quaternary shelf-Margin deltas, northwest Gulf of Mexico: *American Association of Petroleum Geologists, Bulletin*, v. 69, p. 77-91.

Thompson, W.G., and Goldstein, S.L., 2005, Open system coral ages reveal persistent suborbital sea-level cycles: *Science*, v. 308, no. 5720, p. 401-404, doi: 0.1126/science.1104035.

Thunell, R., Tappa, E., Pride, C., and Kincaid, E., 1999, Sea-surface temperature anomalies associated with the 1997-1998 El Nino recorded in the oxygen isotope composition of planktonic foraminifera: *Geology*, v. 27, p. 843-846.

Wilkinson, B.H., and Algeo, T.J., 1989, Sedimentary carbonate record of calcium-magnesium cycling. *Am. J. Sci.*, 289:1158-1194.

Williams, D.F., 1984, Correlation of Pleistocene Marine Sediments of the Gulf of Mexico and Other Basins Using Oxygen Isotope Stratigraphy, in *Principles of Pleistocene Stratigraphy*, edited by N. Healy-Williams, p. 65-118, Int. Human Resour. Dev. Corp., Boston, Mass.

Figures

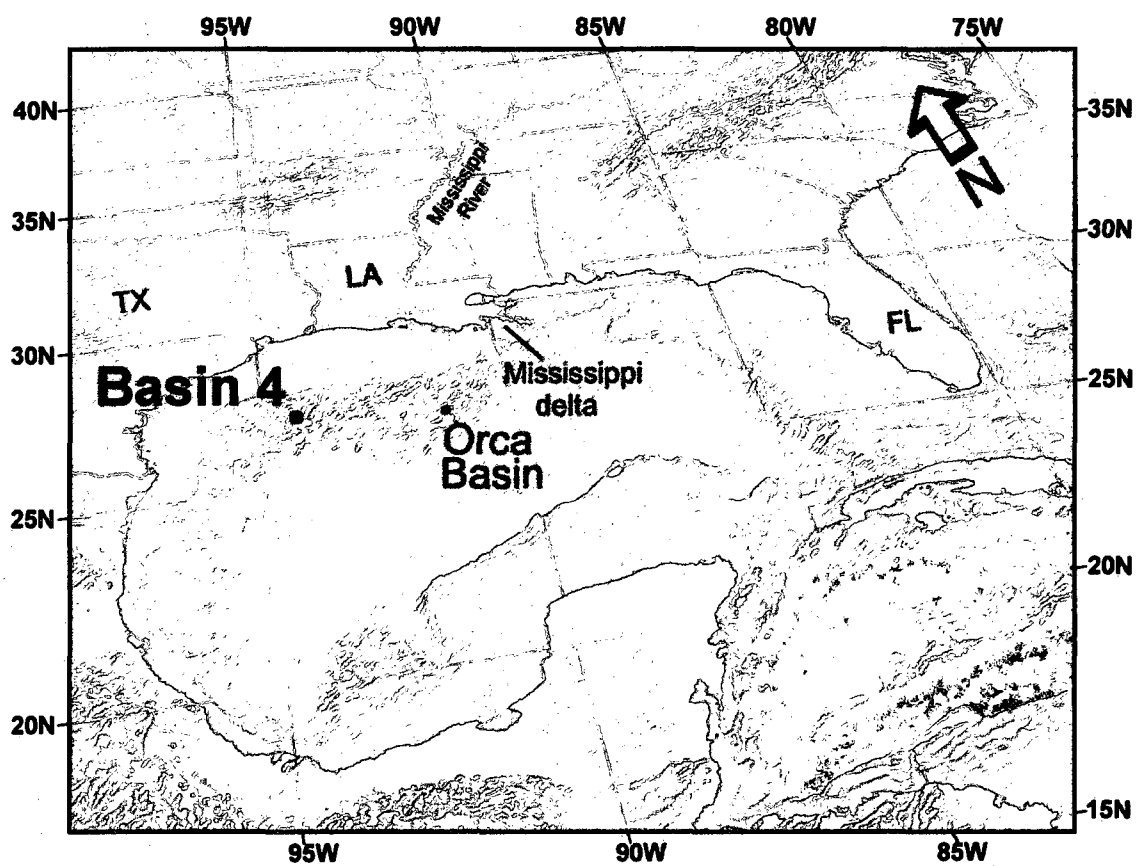


Figure 1.1. Map of the Gulf of Mexico showing the location of Basin 4 and the Orca Basin. This figure is modified from <http://ocean.explorer.noaa.gov>.

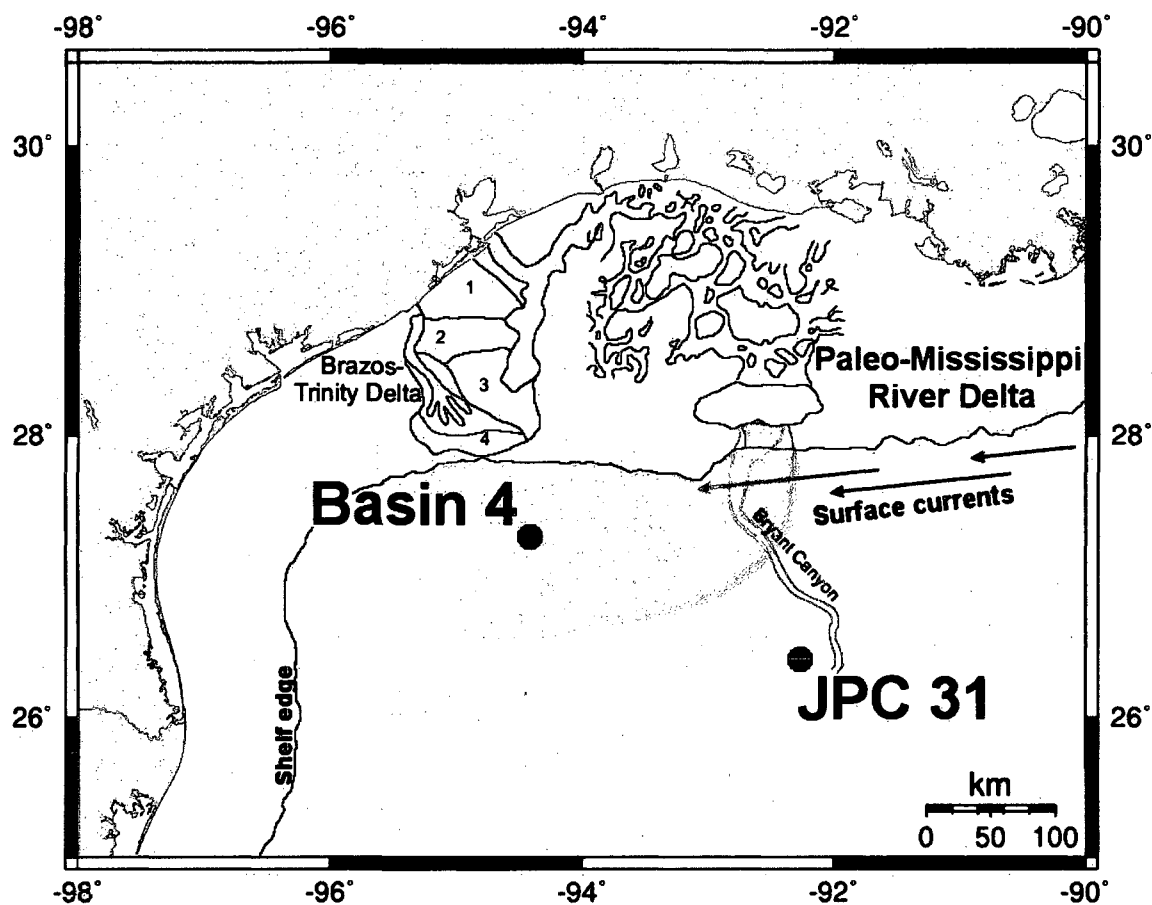


Figure 1.2. Late Pleistocene paleogeographic map of the northwest Gulf of Mexico, showing locations of Basin 4 and Bryant Canyon cores in relation to the two main depositional systems influencing the area. The Mississippi River Delta during Termination II and late MIS 6 (Mississippi River delta information from Tripsanas et al., 2007), and the Brazos-Trinity (B-T) Delta during MIS 5 – MIS 2 (B-T delta information from Anderson et al., 2004). Numbered lobes in the B-T delta indicate chronological order of lobe formation. Prevailing surface currents in this part of the gulf explain the reason for the sensitivity of Basin 4 to meltwater fluxes and large volumes of fine sediment from the Mississippi River during MIS 6. From MIS 5 to MIS 2 the Brazos-Trinity system became the dominant influence on Basin 4 (Mallarino et al., 2006).

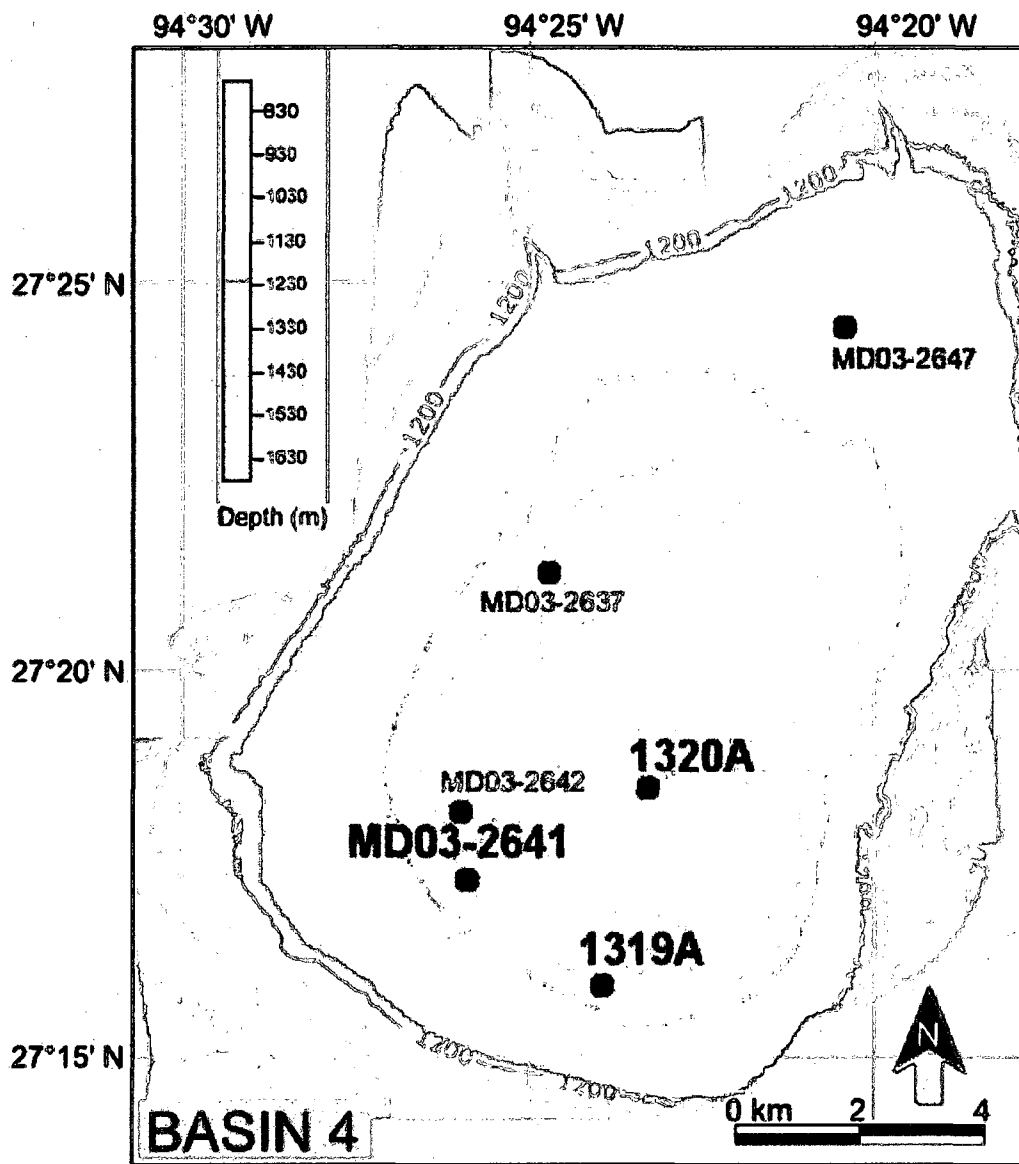


Figure 1.3. A bathymetric map with the location for the three Basin 4 cores. The map is modified from Mallarino et al. (2006).

Table 1.1 Location and depth information for cores used in this study. Information for 1319A and 1320A from Flemings et al., 2006 information for MD03-2641 from Laj (2006).

Core	Total Cored Section (m)	Latitude	Longitude	Water Depth (m)	Environment
1319A	157.5	27°15.9751 N	94°24.1908 W	1429.6	Basin slope
1320A	299.6	27°18.0809 N	94°23.2537 W	1480.4	Basin floor
MD03-2641	39.6	27°17.352 N	94°25.902 W	1427	Basin slope

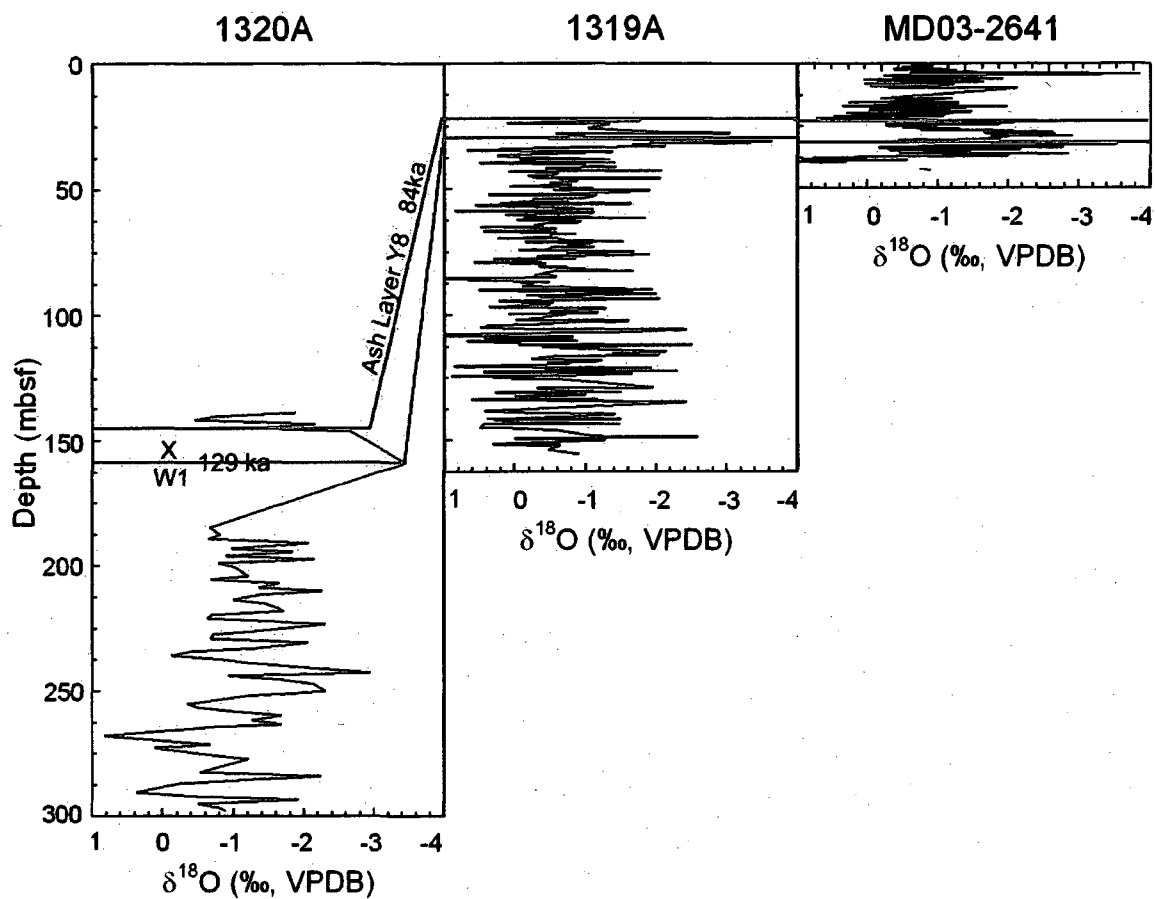


Figure 1.4a. Planktonic $\delta^{18}\text{O}$ records based upon *Globigerinoides ruber* for Basin 4 cores annotated with correlations of the ash layer Y8 and *G. menardii* zone X/W1 boundary.

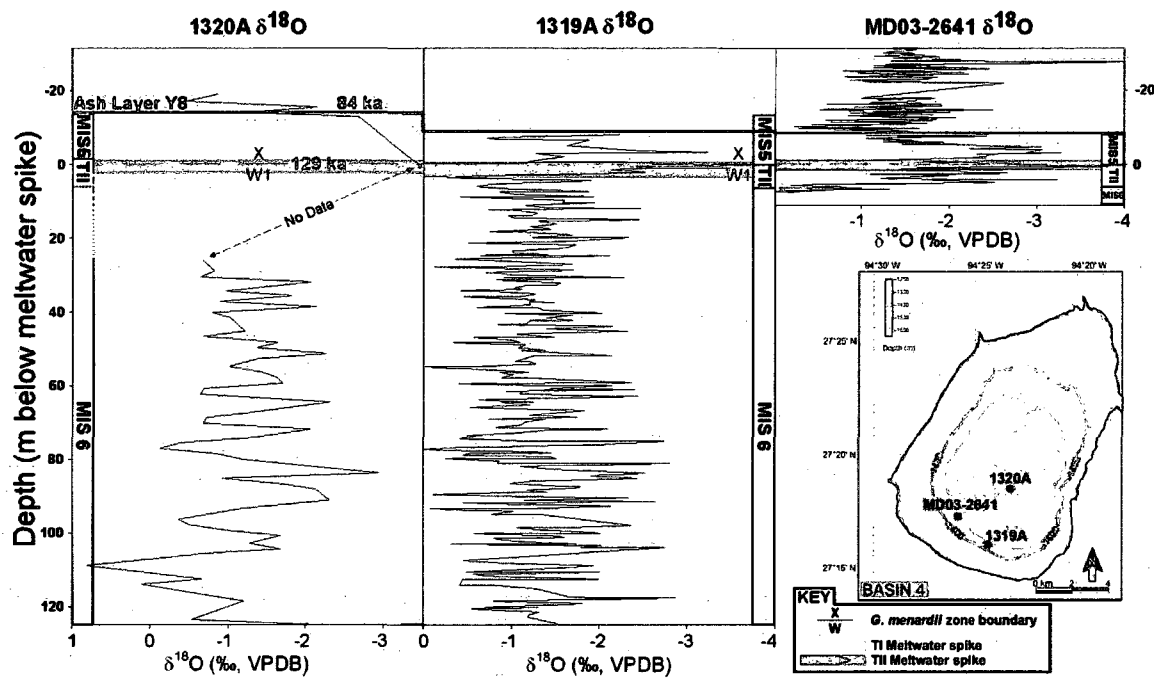


Figure 1.4b. Planktic $\delta^{18}\text{O}$ records for Basin 4 cores, depth corrected to zero at the lightest meltwater peak in each record. Also, a Basin 4 bathymetric map with core locations (modified from Mallarino et al., 2006).

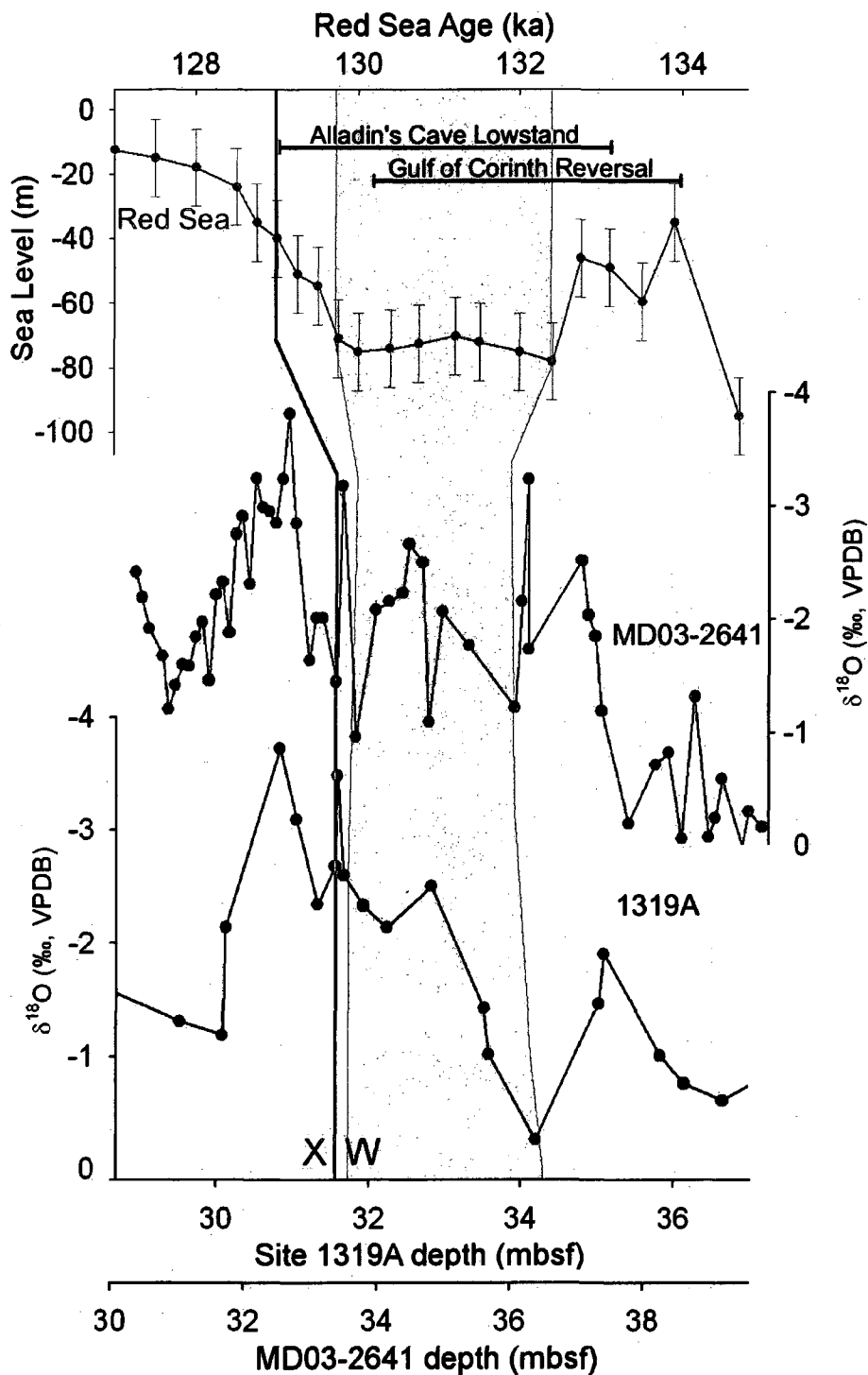


Figure 1.5. TII climate reversal (gray shaded area) observed in $\delta^{18}\text{O}$ record of planktonic foraminifer *G. ruber* (white variety) cores 1319A and MD03-2641. *G. menardii* zone boundary (red line) seen in cores 1319A and MD03-2641, dated to approximately 129 ka (Kennett and Huddleston, 1972). Correlation to Red Sea data, from Siddall et al. (2007), Aladdin's Cave data from McCulloch and Esat (1999), and Gulf of Corinth data from Andrews et al. (2007).

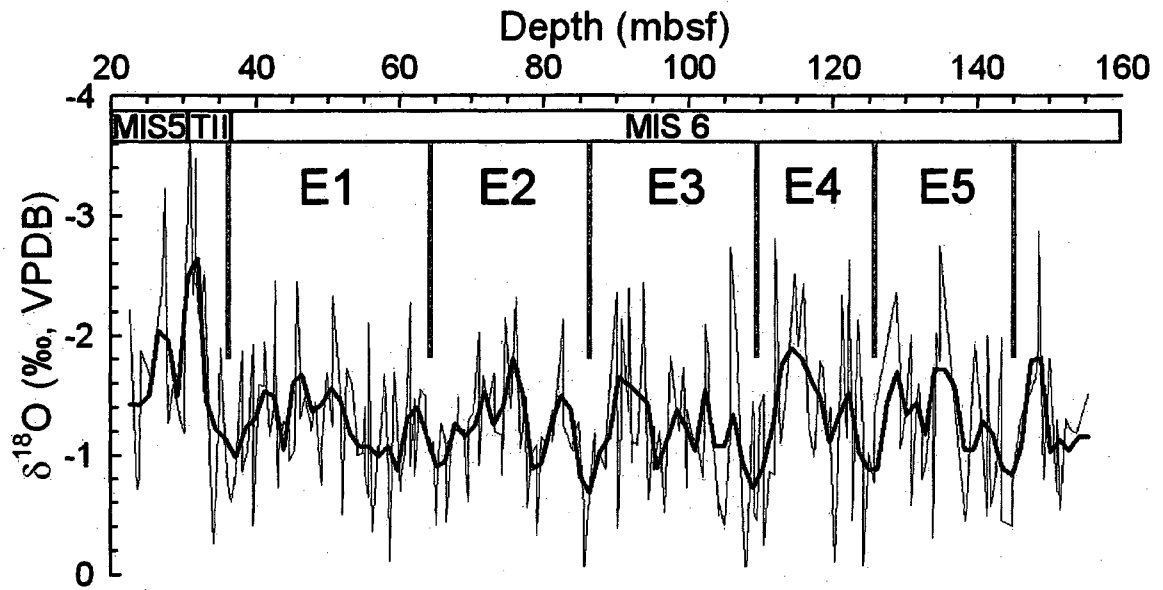


Figure 1.6. $\delta^{18}\text{O}$ on *G. ruber* (white) from Basin 4 core 1319A. All *G. ruber* $\delta^{18}\text{O}$ measurements for core 1319A, shown with five-point smooth fit, and segmented into E-events referred to in the text.

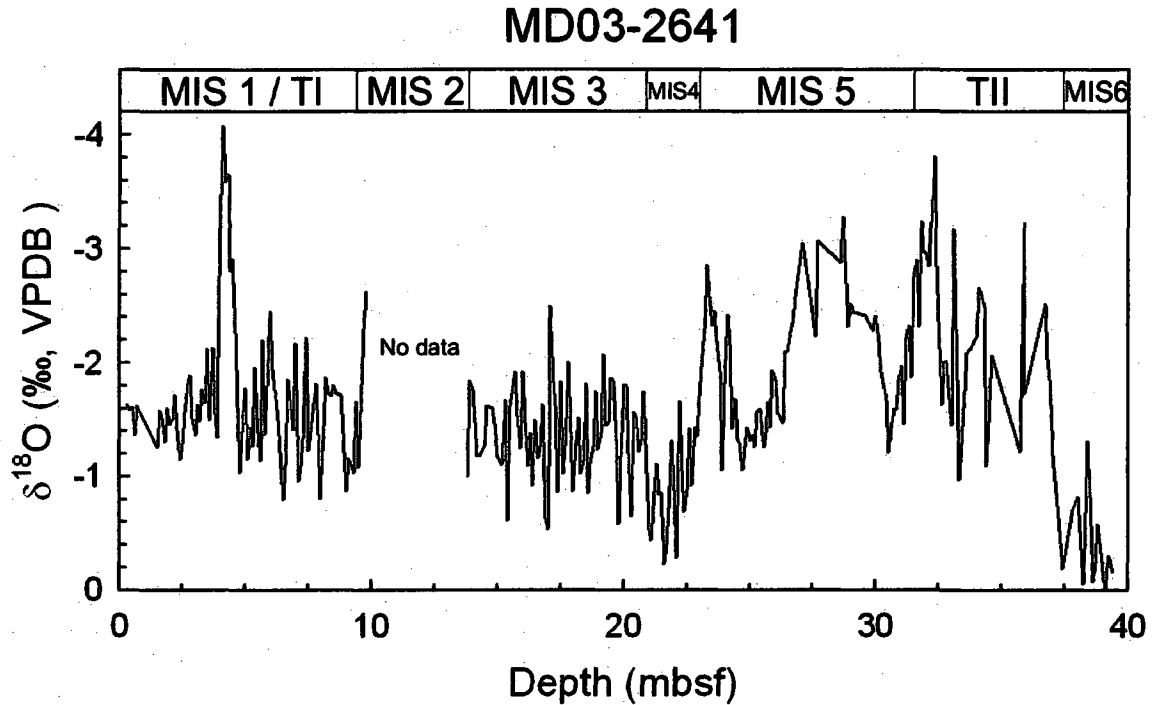


Figure 1.7. $\delta^{18}\text{O}$ record of planktonic foraminifera *G. ruber* in Basin 4, core MD03-2641. This record is important for using its MIS 3 climate oscillations from 21 to 14 mbsf, and the TI meltwater spike at 4 mbsf for comparing to older $\delta^{18}\text{O}$ high amplitude variations observed in the other two sedimentary sequences analyzed in this study.

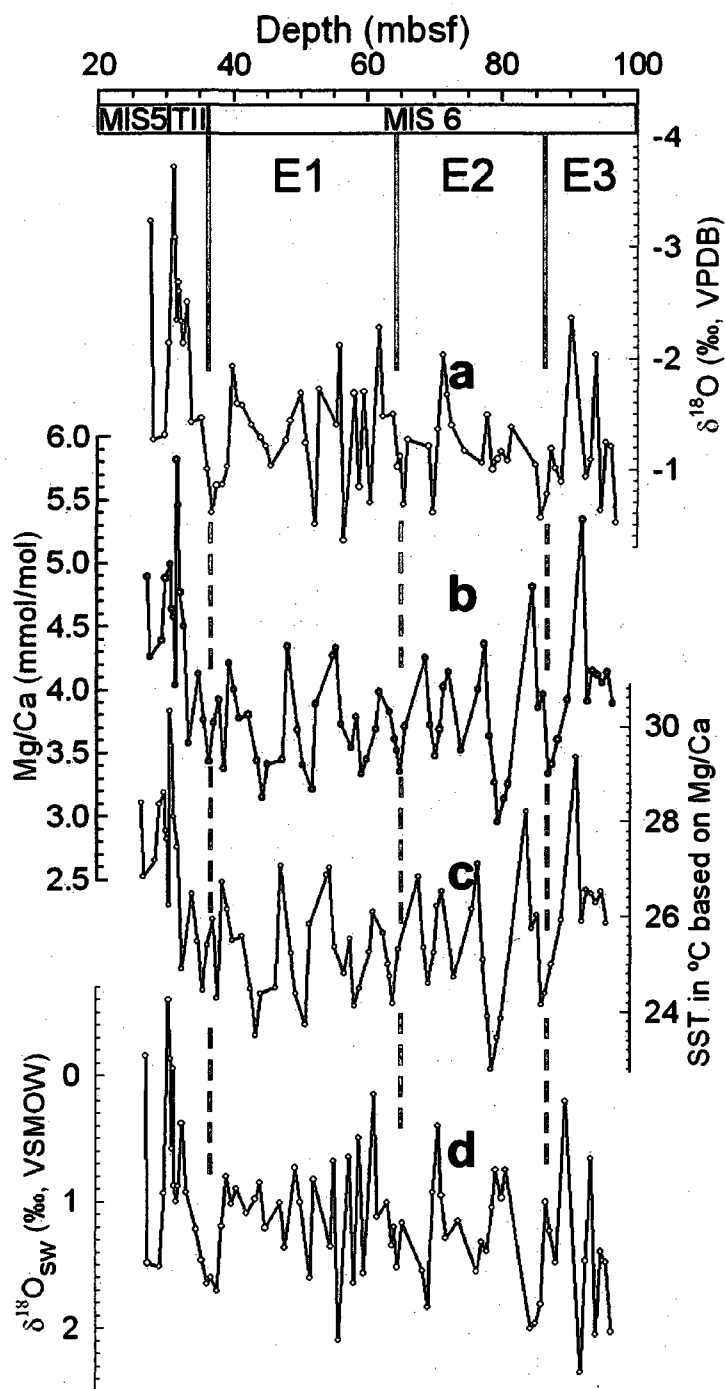


Figure 1.8. MIS 6/TII climate proxy records from Hole 1319A. Events E1 to E3, earlier identified in the high resolution $\delta^{18}\text{O}$ data (Figure 5), are shown. Sample spacing is generally every 75 cm, except from 30 to 32 mbsf, where sample spacing can be as narrow as 30 cm. (a) $\delta^{18}\text{O}$ values measured from *G. ruber* (white variety). (b) Mg/Ca data versus depth in core. (c) Sea surface temperature calculated from Mg/Ca ratios. (d) $\delta^{18}\text{O}_{\text{seawater}}$ after subtracting out the temperature effect and converting to VSMOW. Total error in calculating $\delta^{18}\text{O}_{\text{sw}}$ is $\pm 3.1\%$ or less than $\pm 0.06\%$. For errors in previous calculations refer to Methods.

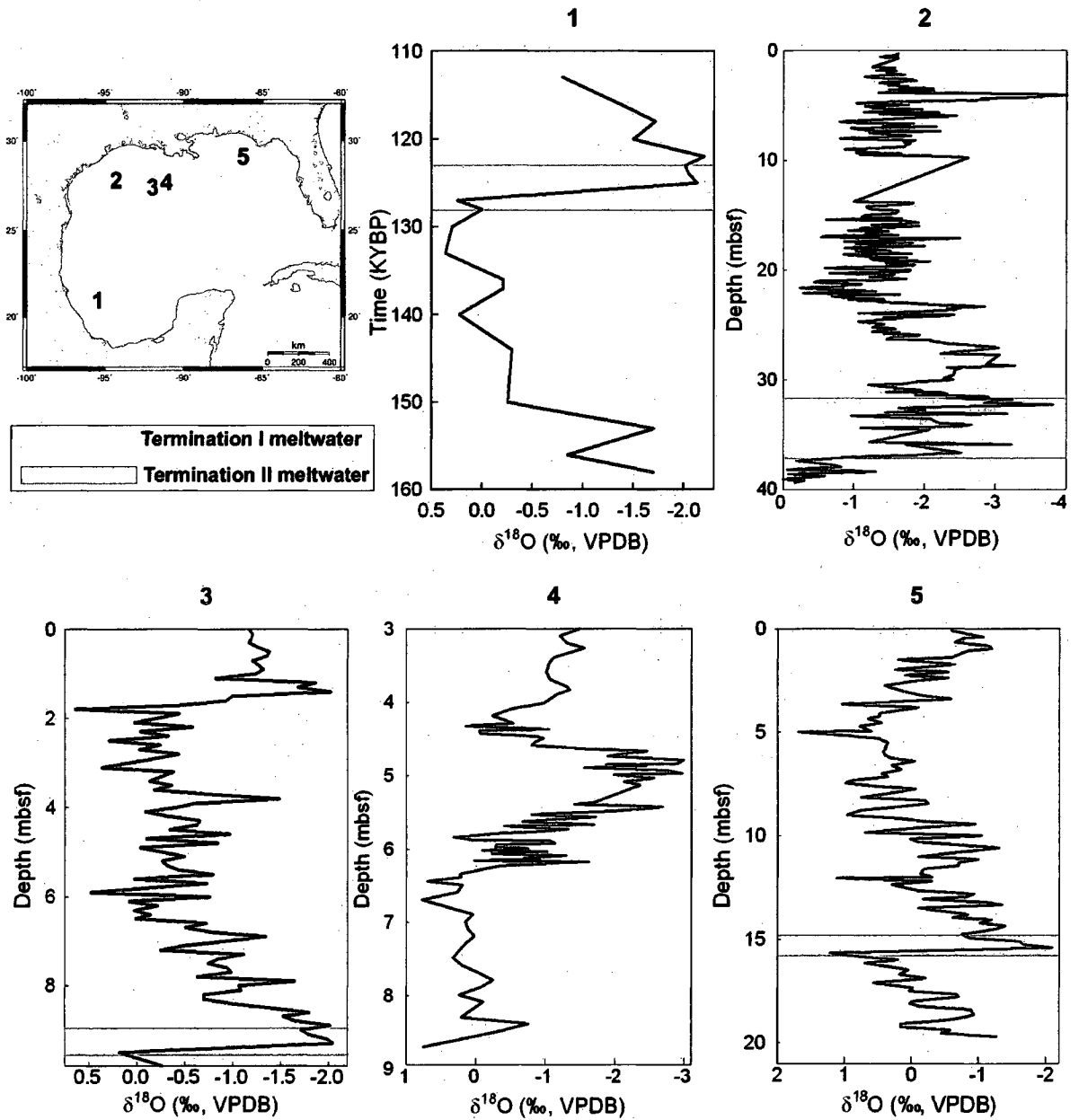


Figure 1.9. Termination I and II $\delta^{18}\text{O}$ meltwater responses in planktonic foraminifers throughout the Gulf of Mexico (yellow and blue highlighted areas respectively). Data from each of the cores were taken from the following: core 1, TR126 -23 from Falls, 1980; core 2, MD03-2641 from this study; core 3, JPC-31 from Tripsanas et al., 2007; core 4, EN32-PC6 from Flower, 2004; core 5, ODP 625B from Joyce et al., 1990.

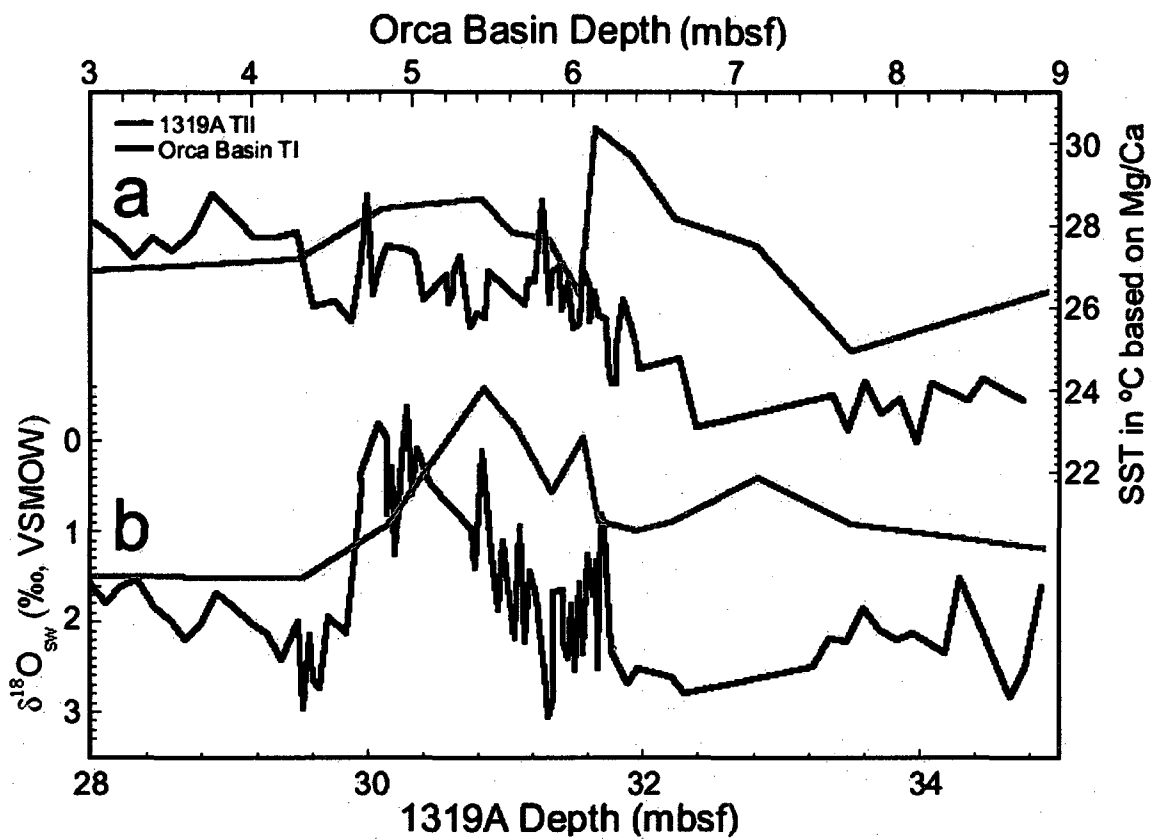


Figure 1.10. $\delta^{18}\text{O}_{\text{sw}}$ and SST curves for TII in 1319A (Basin 4) and TI in the Orca Basin covering comparable meltwater events. The $\delta^{18}\text{O}_{\text{sw}}$ TII signal in 1319A does not show quite the magnitude as the TI event, however the values do fall within the same range as the TI Orca Basin. Temperature changes are also comparable with warming through the meltwater event. Orca Basin values from Flower et al. (2004).

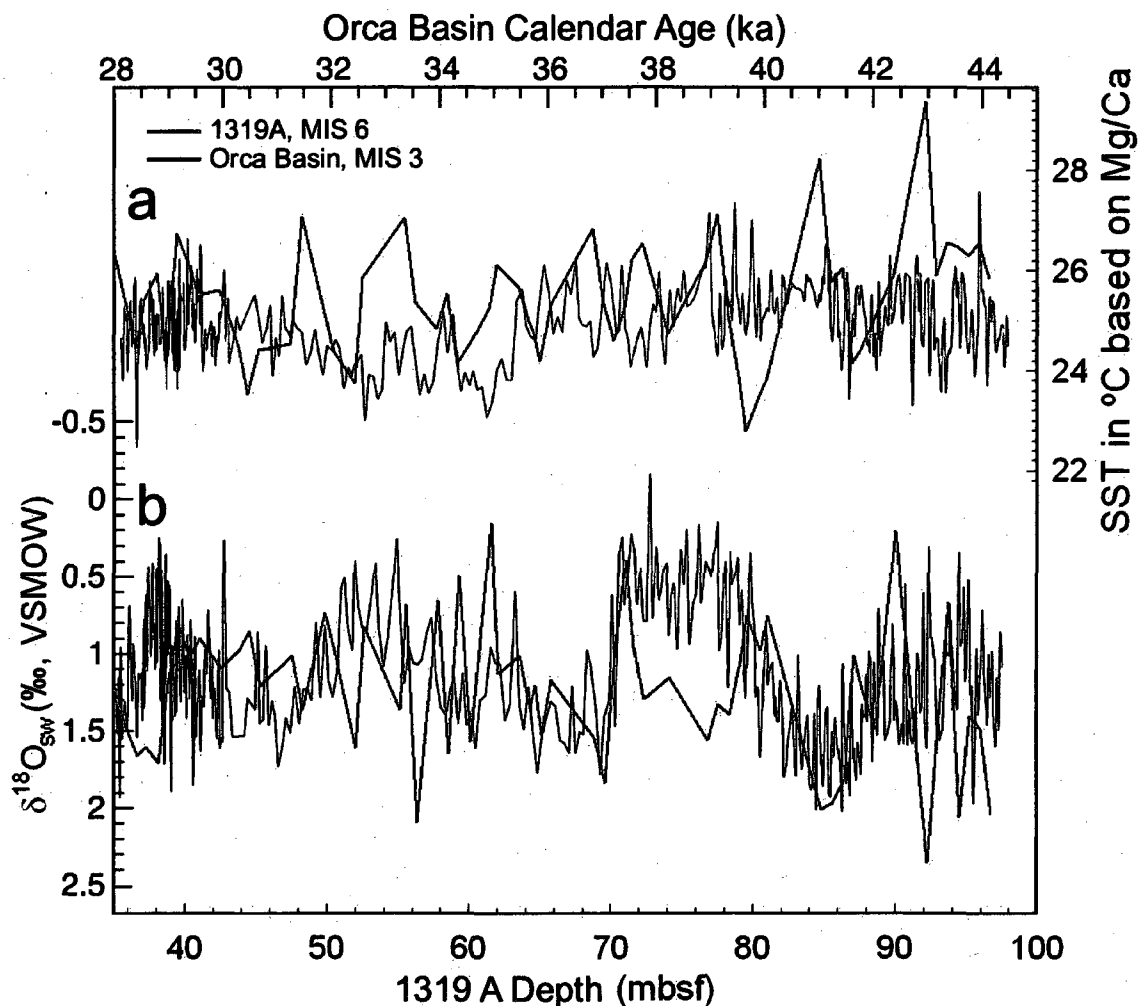


Figure 1.11. $\delta^{18}O_{sw}$ and SST curves for MIS 6 in 1319A (Basin 4) are plotted with respect to depth, and MIS 3 in the Orca Basin, which are plotted with respect to age (ka), cover comparable meltwater events. The values from MIS 6 are generally comparable to those from MIS 3, with some variation in the oldest part of MIS 6. Orca Basin values from Hill et al. (2006).

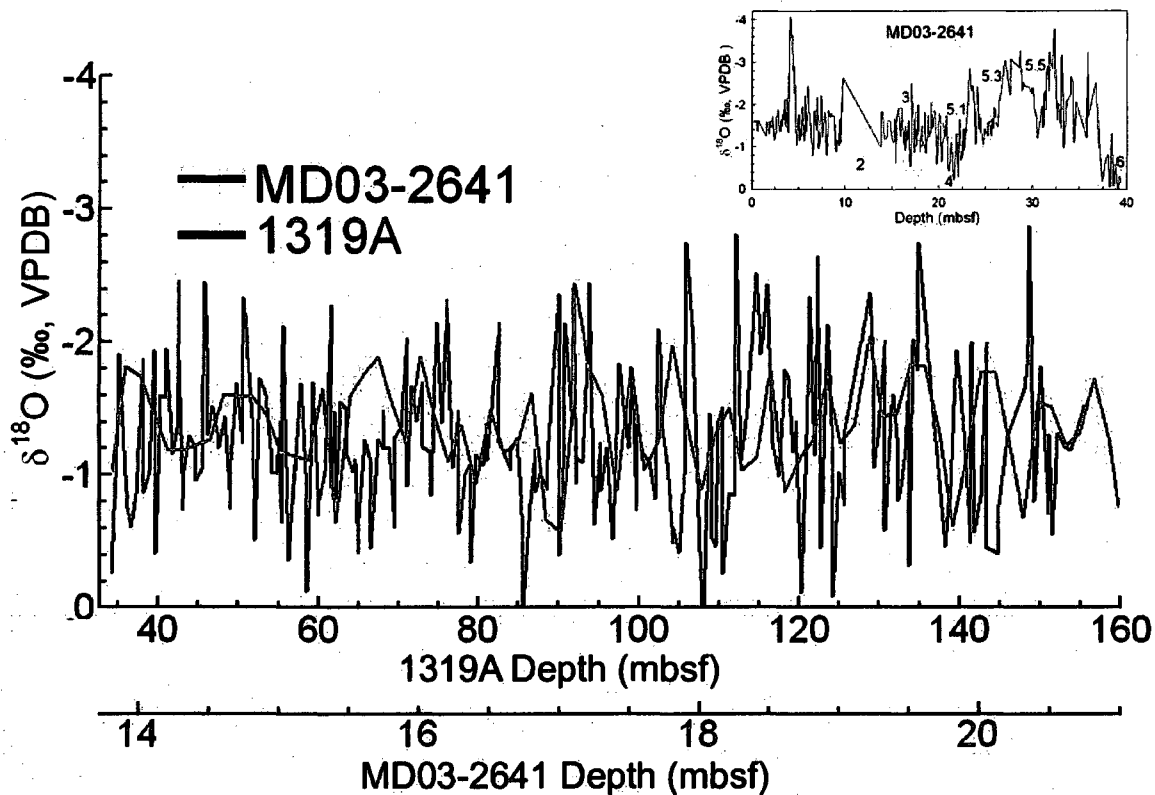


Figure 1.12. $\delta^{18}\text{O}$ on *G. ruber* (white variety) from Basin 4 cores MD03-2641 and 1319A. The MIS 3 record from MD-41 (with clarifying top right corner figure) is overlain on top of the MIS 6 record from 1319A. Amplitudes of anomalous excursions for both time periods are similar to one another. Troughs in 1319A are slightly heavier than MD-41, possibly because MIS 6 is a fully glacial time period.

APPENDIX A. Basin 4 Core Data

Table A.1. Data for Hole U1319A Latitude: 27° 15.9751'N, Longitude: 94° 24.1908'W. Hole, Depth (mbsf), $\delta^{18}\text{O}$ (VPDB) (per mill), $\delta^{13}\text{C}$ (VPDB) (per mill).

Hole	Depth (mbsf)	$\delta^{18}\text{O}$ per mill	$\delta^{13}\text{C}$ per mill	Hole	Depth (mbsf)	$\delta^{18}\text{O}$ per mill	$\delta^{13}\text{C}$ per mill	Hole	Depth (mbsf)	$\delta^{18}\text{O}$ per mill	$\delta^{13}\text{C}$ per mill
1319A	22.58	-2.2181	1.1760	1319A	44.58	-0.9587	0.4599	1319A	65.08	-0.4157	0.2297
1319A	23.08	-1.5053	1.6879	1319A	45.32	-1.0416	0.8504	1319A	65.08	-0.6844	0.6188
1319A	23.58	-0.7215	0.9876	1319A	45.67	-2.4505	0.5840	1319A	65.81	-1.2696	0.9881
1319A	23.87	-0.8225	1.2751	1319A	46.07	-1.6985	0.6755	1319A	66.57	-1.1002	-0.3847
1319A	24.09	-1.8732	0.9064	1319A	46.08	-1.3038	0.7284	1319A	66.57	-0.4499	0.8072
1319A	25.59	-1.6372	0.3080	1319A	46.83	-1.5114	0.6496	1319A	67.37	-1.2657	0.9082
1319A	27.09	-2.4520	-0.2710	1319A	47.02	-1.4120	0.9727	1319A	68.05	-1.2041	-0.4770
1319A	27.44	-3.2358	0.3310	1319A	47.56	-1.2664	1.1483	1319A	68.15	-1.4868	0.7891
1319A	27.81	-1.2719	0.6379	1319A	47.58	-1.2060	1.1322	1319A	68.86	-1.2116	0.6474
1319A	28.59	-1.5882	0.7795	1319A	48.31	-1.4428	1.0002	1319A	69.59	-0.6087	0.3773
1319A	29.53	-1.3114	0.8411	1319A	49.08	-0.7449	1.0627	1319A	69.58	-1.2894	-0.3075
1319A	30.09	-1.1863	1.0176	1319A	49.09	-1.1089	1.0633	1319A	70.33	-1.3620	0.2400
1319A	30.13	-2.1366	0.7167	1319A	49.84	-1.6920	0.7803	1319A	71.07	-2.0285	0.2447
1319A	30.84	-3.7207	0.7237	1319A	50.57	-1.2400	0.8525	1319A	71.08	-0.9234	0.0674
1319A	31.06	-3.0889	0.5509	1319A	50.58	-2.3302	1.2769	1319A	71.60	-1.6760	0.6041
1319A	31.33	-2.3402	0.2570	1319A	51.8	-1.4321	0.8416	1319A	71.60	-1.6628	0.7392
1319A	31.56	-2.6798	0.1588	1319A	52.03	-0.5072	0.9260	1319A	72.31	-1.4018	0.5441
1319A	31.59	-3.4816	0.1298	1319A	52.58	-1.7273	0.9464	1319A	73.11	-1.6956	0.7065
1319A	31.67	-2.6016	0.7547	1319A	53.39	-1.6046	0.6301	1319A	73.10	-1.2105	0.4037
1319A	31.93	-2.3318	0.3690	1319A	54.07	-1.0912	1.0821	1319A	74.14	-1.1664	0.8804
1319A	32.24	-2.1362	0.4673	1319A	54.08	-1.0073	0.8612	1319A	74.15	-0.8439	0.3727
1319A	32.83	-2.5042	0.5731	1319A	54.83	-1.0231	1.1274	1319A	74.67	-2.1506	0.8144
1319A	33.52	-1.4240	0.4451	1319A	55.15	-1.4089	1.1243	1319A	75.42	-1.3970	1.1136
1319A	33.59	-1.0135	-0.1426	1319A	55.15	-0.8633	1.0676	1319A	76.11	-2.3264	0.7874
1319A	34.21	-0.2595	0.2226	1319A	55.58	-0.6441	0.6902	1319A	76.10	-2.1452	0.0454
1319A	35.02	-1.4610	0.7746	1319A	55.59	-2.1184	0.4970	1319A	76.79	-1.0582	0.8148
1319A	35.09	-1.9052	0.4985	1319A	56.31	-0.3595	0.9751	1319A	77.59	-1.4902	0.7017
1319A	35.83	-1.0050	0.6340	1319A	57.07	-1.0791	0.9736	1319A	77.60	-0.5638	0.3644
1319A	36.15	-0.7556	0.7429	1319A	57.08	-1.0269	0.5771	1319A	78.34	-0.9999	0.8153
1319A	36.65	-0.6070	0.8121	1319A	57.82	-1.6879	0.6925	1319A	79.09	-1.0927	0.4909
1319A	37.28	-0.8549	0.8989	1319A	58.57	-0.8450	0.7068	1319A	79.10	-0.3382	0.3055
1319A	38.09	-1.8777	0.8968	1319A	58.58	-0.1199	0.1074	1319A	79.60	-1.1591	0.5081
1319A	38.14	-0.8647	0.8859	1319A	59.32	-1.6999	0.8749	1319A	80.52	-1.0794	0.5275
1319A	38.83	-1.0302	1.0484	1319A	60.09	-0.7039	0.8558	1319A	81.09	-1.3836	0.4796
1319A	39.58	-1.9340	1.2458	1319A	60.1	-0.8134	0.5679	1319A	81.10	-1.1109	0.6106
1319A	39.59	-0.4068	0.9450	1319A	60.84	-1.0273	0.9837	1319A	81.84	-1.5988	0.6533
1319A	40.33	-1.5956	0.8191	1319A	61.54	-2.2794	0.7069	1319A	82.59	-2.1447	0.6970
1319A	41.08	-1.5806	0.8101	1319A	61.55	-0.9129	0.8923	1319A	82.60	-1.2535	-0.1138
1319A	41.09	-1.9454	0.8975	1319A	62.08	-1.4806	0.8881	1319A	84.08	-1.0395	0.4913
1319A	41.83	-1.1609	0.4747	1319A	62.085	-0.8286	0.5468	1319A	84.09	-1.1961	0.0948
1319A	42.52	-1.4064	0.1504	1319A	62.83	-1.5562	0.6535	1319A	84.80	-1.2758	0.7911
1319A	42.6	-2.4617	0.6721	1319A	63.58	-1.5011	0.9695	1319A	85.57	-0.5646	-0.6501
1319A	42.59	-1.8613	0.5515	1319A	63.585	-1.1583	0.6666	1319A	85.58	-0.0166	0.2628
1319A	43.08	-0.7331	0.2989	1319A	64.31	-1.0282	1.0194	1319A	86.40	-0.7772	0.5956
1319A	43.09	-1.0338	0.6019	1319A	64.66	-1.1200	0.7190	1319A	87.09	-0.8698	0.1434
1319A	43.84	-1.2932	0.7827	1319A	64.65	-1.0894	0.3055	1319A	87.10	-1.1906	0.4910

Hole	Depth (mbsf)	$\delta^{18}\text{O}$ per mill	$\delta^{13}\text{C}$ per mill	Hole	Depth (mbsf)	$\delta^{18}\text{O}$ per mill	$\delta^{13}\text{C}$ per mill	Hole	Depth (mbsf)	$\delta^{18}\text{O}$ per mill	$\delta^{13}\text{C}$ per mill
1319A	87.67	-1.0156	0.5239	1319A	111.18	-0.8664	0.3958	1319A	134.78	-2.7485	0.4090
1319A	88.58	-0.8890	0.8848	1319A	111.93	-0.8438	0.2582	1319A	138.32	-0.4582	0.7254
1319A	88.57	-1.1165	0.6324	1319A	111.93	-2.8111	0.0422	1319A	138.88	-0.9099	0.7954
1319A	89.99	-2.3591	0.7211	1319A	112.68	-1.1099	0.3470	1319A	139.63	-1.9331	0.7515
1319A	90.16	-0.3932	0.3542	1319A	113.43	-1.4938	0.4519	1319A	140.38	-1.4676	0.5007
1319A	90.7	-1.2691	0.4446	1319A	114.62	-2.5188	0.1538	1319A	141.45	-0.4880	0.4488
1319A	90.71	-2.1383	0.3191	1319A	115.18	-1.9140	0.5505	1319A	141.45	-2.0056	0.9301
1319A	91.78	-1.3752	0.8243	1319A	115.93	-2.4365	0.3740	1319A	141.88	-0.5718	0.1462
1319A	91.77	-2.4007	1.2290	1319A	116.68	-1.2384	0.5454	1319A	142.63	-0.8408	1.0898
1319A	92.2	-0.9363	0.2839	1319A	117.40	-0.9882	0.3478	1319A	143.37	-1.9909	0.6158
1319A	92.2	-1.1270	0.5704	1319A	118.18	-1.7137	0.4754	1319A	143.38	-0.4538	0.6010
1319A	92.95	-1.0894	0.4227	1319A	118.18	-1.7934	0.4305	1319A	144.88	-0.4068	0.1565
1319A	93.69	-2.0318	0.6486	1319A	118.62	-1.7251	0.4902	1319A	144.89	-0.7680	0.5278
1319A	93.7	-2.4436	0.8559	1319A	119.18	-1.1781	0.8119	1319A	145.88	-1.2977	0.9773
1319A	94.45	-0.6264	0.7973	1319A	119.69	-1.4042	1.2111	1319A	148.00	-1.6439	0.6182
1319A	95.19	-1.2445	0.6995	1319A	119.69	-1.1629	0.3065	1319A	148.48	-1.9165	0.7960
1319A	95.2	-0.8810	-0.0898	1319A	120.29	-0.1109	0.5278	1319A	148.48	-2.8746	0.4217
1319A	95.94	-1.2065	0.6808	1319A	121.18	-1.9026	0.1073	1319A	149.23	-0.8004	0.6637
1319A	96.7	-0.5187	0.5516	1319A	121.18	-2.3408	0.4705	1319A	149.97	-1.8136	1.0208
1319A	97.45	-1.8329	0.4113	1319A	121.93	-1.1511	0.7537	1319A	151.05	-0.7045	0.8460
1319A	98.64	-1.2047	0.3258	1319A	122.24	-2.6415	0.3267	1319A	151.05	-1.3024	0.4892
1319A	99.2	-1.7411	0.8004	1319A	122.24	-2.1141	0.8837	1319A	151.50	-0.5487	0.3836
1319A	99.79	-0.7329	0.2857	1319A	122.68	-1.3004	-0.1415	1319A	152.20	-1.3100	0.9623
1319A	99.78	-1.3813	0.1447	1319A	122.68	-0.4554	0.4457	1319A	153.00	-1.2117	0.6413
1319A	100.53	-1.1608	1.0004	1319A	123.45	-2.1337	0.4052	1319A	153.75	-1.1888	0.8073
1319A	101.28	-1.1029	0.4300	1319A	124.18	-1.1867	1.1214	1319A	155.42	-1.5276	0.1885
1319A	102.01	-0.8227	0.4558	1319A	124.18	-0.0809	0.1762				
1319A	102.35	-1.6383	0.2224	1319A	124.92	-1.0240	0.9491				
1319A	102.36	-2.0934	0.4614	1319A	125.68	-0.7757	0.5252				
1319A	102.78	-1.8141	0.7956	1319A	125.68	-1.3447	1.3603				
1319A	102.79	-1.4049	0.4736	1319A	128.77	-2.3647	0.5239				
1319A	103.53	-1.0972	0.9426	1319A	129.27	-1.7014	0.9618				
1319A	104.31	-0.4905	0.3245	1319A	129.28	-1.0618	0.6385				
1319A	104.3	-0.6000	0.4588	1319A	130.02	-1.3535	1.3230				
1319A	105.06	-0.4195	0.2220	1319A	130.78	-2.0136	0.6529				
1319A	105.78	-1.1559	0.3903	1319A	130.78	-0.5790	0.7541				
1319A	105.79	-2.7408	0.5922	1319A	131.53	-1.4478	0.6686				
1319A	106.72	-1.9962	0.8212	1319A	131.83	-1.6047	1.0956				
1319A	107.58	-0.4282	0.6957	1319A	132.28	-1.1792	0.6377				
1319A	108.03	0.0771	0.0207	1319A	132.28	-0.8075	0.6801				
1319A	108.87	-1.4573	-0.1980	1319A	132.88	-0.9619	0.9980				
1319A	109.1	-1.2734	0.4992	1319A	133.27	-1.1948	0.7370				
1319A	109.11	-0.5286	0.0197	1319A	133.77	-1.7342	0.7823				
1319A	109.53	-0.4574	0.2558	1319A	133.78	-0.3122	-0.1051				
1319A	109.87	-1.4046	0.1022	1319A	134.23	-2.0239	0.8485				
1319A	110.44	-0.2563	0.8755	1319A	134.77	-1.7943	1.0919				

Table A.2. Data for Hole U1320A Latitude: 27° 18.0809'N, Longitude: 94° 23.2537'W. Hole, Depth (mbsf), $\delta^{18}\text{O}$ (VPDB) (per mill), $\delta^{13}\text{C}$ (VPDB) (per mill).

Hole	Depth (mbsf)	$\delta^{18}\text{O}$ per mill	$\delta^{13}\text{C}$ per mill	Hole	Depth (mbsf)	$\delta^{18}\text{O}$ per mill	$\delta^{13}\text{C}$ per mill
1320A	138.82	-1.8787	1.2689	1320A	258.1	-0.9907	0.3485
1320A	140.29	-0.7381	0.9488	1320A	259.6	-1.6766	0.5204
1320A	141.8	-0.4497	0.9955	1320A	261.7	-1.2776	0.3721
1320A	143.28	-2.1487	1.1789	1320A	263.2	-1.6774	0.6038
1320A	144.79	-1.3069	0.9701	1320A	264.24	-0.7431	1.0470
1320A	146.19	-2.6640	0.9197	1320A	267.7	0.8217	0.2338
1320A	158.79	-3.4591	0.7364	1320A	271.3	-0.6647	0.0836
1320A	184.72	-0.6708	0.7561	1320A	272.8	0.1090	0.0704
1320A	187.72	-0.8185	0.5091	1320A	275.8	-0.7878	0.5898
1320A	189.22	-0.6459	1.1187	1320A	277.31	-1.2063	0.4741
1320A	190.72	-2.0673	0.6668	1320A	282.38	-0.5320	-0.4595
1320A	193.22	-0.9739	0.7666	1320A	283.88	-2.2402	0.3656
1320A	194.39	-1.8354	0.1726	1320A	285.38	-1.2893	0.5720
1320A	195.88	-0.8969	0.2611	1320A	286.93	-0.2338	-0.0456
1320A	197.39	-2.1446	0.8090	1320A	290.49	0.3754	0.0074
1320A	198.88	-0.8005	0.9359	1320A	291.99	-0.4714	0.3948
1320A	200.38	-1.0304	0.4041	1320A	293.04	-1.6063	-0.7205
1320A	203.98	-1.2134	0.7463	1320A	293.49	-1.9165	0.6852
1320A	205.48	-0.6774	0.8380	1320A	294.98	-0.5051	0.2168
1320A	206.98	-1.6393	0.8531	1320A	296.51	-0.7955	0.7515
1320A	208.49	-1.3746	1.0005	1320A	297.98	-0.8906	0.2317
1320A	209.99	-2.2671	0.8145				
1320A	211.48	-1.3792	1.0373				
1320A	213.58	-1.0072	0.6241				
1320A	215.08	-1.4438	0.7584				
1320A	216.58	-1.6329	0.8080				
1320A	218.08	-1.7085	0.5552				
1320A	219.58	-0.6911	0.4283				
1320A	221.08	-0.6386	0.4263				
1320A	223.18	-2.3130	-0.1700				
1320A	225.99	-1.3081	0.6899				
1320A	227.49	-0.7113	0.2976				
1320A	228.99	-0.6771	0.2222				
1320A	230.49	-2.0591	0.6485				
1320A	232.78	-1.3303	0.5628				
1320A	234.28	-0.3899	0.4328				
1320A	235.78	-0.1254	-0.0274				
1320A	237.28	-0.8550	0.2991				
1320A	238.78	-1.2001	0.5738				
1320A	242.48	-2.9534	0.3739				
1320A	243.98	-0.9305	0.6871				
1320A	245.48	-1.7119	0.7398				
1320A	246.98	-2.1372	0.1218				
1320A	249.91	-2.3093	0.5518				
1320A	252.1	-1.1774	0.6083				
1320A	255.1	-0.3611	0.4240				
1320A	256.6	-0.4941	0.0394				

Table A.3. Data for MD03-2641, Basin 4, Latitude: 27° 17.352'N, Longitude: 94° 25.902'W. Hole, Depth (mbsf), $\delta^{18}\text{O}$ (VPDB) (per mill).

Hole	Depth (mbsf)	$\delta^{18}\text{O}$ (VPDB) (per mill)	Hole	Depth (mbsf)	$\delta^{18}\text{O}$ (VPDB) (per mill)	Hole	Depth (mbsf)	$\delta^{18}\text{O}$ (VPDB) (per mill)
MD03-2641	0.3	-1.62946	MD03-2641	5.7	-2.2057119	MD03-2641	15.8	-1.5388505
MD03-2641	0.4	-1.5869861	MD03-2641	5.8	-1.3694222	MD03-2641	15.9	-1.2519916
MD03-2641	0.5	-1.6144119	MD03-2641	6	-2.4565951	MD03-2641	16	-1.926632
MD03-2641	0.6	-1.365796	MD03-2641	6.1	-1.9444712	MD03-2641	16.1	-1.4822506
MD03-2641	0.7	-1.6279004	MD03-2641	6.3	-1.4989124	MD03-2641	16.2	-1.0904937
MD03-2641	1.5	-1.2578348	MD03-2641	6.5	-0.79310601	MD03-2641	16.3	-1.3807937
MD03-2641	1.6	-1.5816119	MD03-2641	6.6	-1.0922647	MD03-2641	16.4	-0.92579632
MD03-2641	1.7	-1.5160129	MD03-2641	6.7	-1.8564487	MD03-2641	16.5	-1.4967052
MD03-2641	1.8	-1.311053	MD03-2641	6.9	-1.4071503	MD03-2641	16.6	-1.165793
MD03-2641	1.9	-1.6038466	MD03-2641	7	-2.1702826	MD03-2641	16.7	-1.2614053
MD03-2641	2	-1.456989	MD03-2641	7.1	-0.95915871	MD03-2641	16.8	-1.630796
MD03-2641	2.1	-1.5120996	MD03-2641	7.2	-1.0937675	MD03-2641	16.9	-0.63506442
MD03-2641	2.2	-1.7170783	MD03-2641	7.3	-1.3366153	MD03-2641	17	-0.53175383
MD03-2641	2.3	-1.4080891	MD03-2641	7.4	-2.222799	MD03-2641	17.1	-1.6419265
MD03-2641	2.4	-1.1479791	MD03-2641	7.5	-1.2269005	MD03-2641	17.1	-2.5041064
MD03-2641	2.5	-1.2839707	MD03-2641	7.8	-1.8127098	MD03-2641	17.2	-1.8348154
MD03-2641	2.6	-1.5616047	MD03-2641	7.9	-1.373873	MD03-2641	17.3	-1.6211733
MD03-2641	2.7	-1.8181355	MD03-2641	8	-0.80741333	MD03-2641	17.4	-0.86071115
MD03-2641	2.8	-1.8889896	MD03-2641	8.2	-1.8707367	MD03-2641	17.5	-1.8395009
MD03-2641	2.9	-1.5216723	MD03-2641	8.3	-1.7398607	MD03-2641	17.6	-1.0314293
MD03-2641	3	-1.3605618	MD03-2641	8.4	-1.7074094	MD03-2641	17.7	-1.2684744
MD03-2641	3.1	-1.6370031	MD03-2641	8.5	-1.8041339	MD03-2641	17.8	-2.0117685
MD03-2641	3.2	-1.4854279	MD03-2641	8.6	-1.7400763	MD03-2641	17.9	-1.3916841
MD03-2641	3.3	-1.7648658	MD03-2641	8.8	-1.7161859	MD03-2641	18	-0.8728488
MD03-2641	3.4	-1.6490325	MD03-2641	9	-0.87321013	MD03-2641	18.1	-1.2883479
MD03-2641	3.5	-2.1264842	MD03-2641	9.1	-1.1610379	MD03-2641	18.2	-1.517878
MD03-2641	3.6	-1.4950655	MD03-2641	9.3	-1.0351303	MD03-2641	18.3	-1.0284831
MD03-2641	3.7	-2.1319493	MD03-2641	9.4	-1.666319	MD03-2641	18.4	-1.1367215
MD03-2641	3.8	-1.5595734	MD03-2641	9.5	-1.0897531	MD03-2641	18.5	-1.8184074
MD03-2641	3.9	-1.3429598	MD03-2641	9.7	-2.293599	MD03-2641	18.6	-0.85263929
MD03-2641	4	-3.472135	MD03-2641	9.8	-2.6253899	MD03-2641	18.7	-1.1178317
MD03-2641	4.1	-4.0767693	MD03-2641	13.8	-0.99605196	MD03-2641	18.8	-1.2586579
MD03-2641	4.2	-3.5884585	MD03-2641	13.9	-1.8436199	MD03-2641	18.9	-1.750495
MD03-2641	4.3	-3.6576861	MD03-2641	14	-1.7709431	MD03-2641	19	-1.2426647
MD03-2641	4.4	-2.8049832	MD03-2641	14.2	-1.1823563	MD03-2641	19.1	-1.3848877
MD03-2641	4.5	-2.9136198	MD03-2641	14.3	-1.1819049	MD03-2641	19.2	-2.078637
MD03-2641	4.6	-2.2655706	MD03-2641	14.5	-1.2646278	MD03-2641	19.3	-1.449614
MD03-2641	4.7	-1.6160422	MD03-2641	14.6	-1.6268466	MD03-2641	19.4	-1.4774413
MD03-2641	4.8	-1.034552	MD03-2641	14.8	-1.6039308	MD03-2641	19.5	-1.8661177
MD03-2641	4.9	-1.571979	MD03-2641	14.9	-1.4705151	MD03-2641	19.6	-1.8494928
MD03-2641	5	-1.777216	MD03-2641	15	-1.1723505	MD03-2641	19.7	-1.3273522
MD03-2641	5.1	-1.1489544	MD03-2641	15.2	-1.1009672	MD03-2641	19.8	-0.58590189
MD03-2641	5.2	-1.43176	MD03-2641	15.3	-1.6750958	MD03-2641	19.9	-1.1698122
MD03-2641	5.3	-1.2641502	MD03-2641	15.4	-0.61063528	MD03-2641	20	-1.8097255
MD03-2641	5.4	-1.9584786	MD03-2641	15.5	-1.6123357	MD03-2641	20.1	-1.7945565
MD03-2641	5.5	-1.5140117	MD03-2641	15.6	-1.7879197	MD03-2641	20.2	-1.2138404
MD03-2641	5.6	-1.1429583	MD03-2641	15.7	-1.9193843	MD03-2641	20.3	-0.65283505

Hole	Depth (mbsf)	$\delta^{18}\text{O}$ (VPDB) (per mill)	Hole	Depth (mbsf)	$\delta^{18}\text{O}$ (VPDB) (per mill)	Hole	Depth (mbsf)	$\delta^{18}\text{O}$ (VPDB) (per mill)
MD03-2641	20.4	-1.5698965	MD03-2641	25.1	-1.3658917	MD03-2641	32.1	-2.8471532
MD03-2641	20.5	-1.5316564	MD03-2641	25.2	-1.2551471	MD03-2641	32.2	-3.2338622
MD03-2641	20.6	-1.2206191	MD03-2641	25.3	-1.5651196	MD03-2641	32.3	-3.813805
MD03-2641	20.7	-1.3163456	MD03-2641	25.4	-1.5926418	MD03-2641	32.4	-2.8460613
MD03-2641	20.8	-1.748122	MD03-2641	25.5	-1.3689732	MD03-2641	32.6	-1.6359432
MD03-2641	20.9	-1.2837934	MD03-2641	25.6	-1.2586975	MD03-2641	32.7	-2.0104104
MD03-2641	21	-0.5317829	MD03-2641	25.7	-1.6531008	MD03-2641	32.8	-2.0121929
MD03-2641	21.1	-0.43936876	MD03-2641	25.8	-1.4305539	MD03-2641	33	-1.4506879
MD03-2641	21.2	-0.73343471	MD03-2641	25.9	-1.9364142	MD03-2641	33.1	-3.1750616
MD03-2641	21.3	-1.1092498	MD03-2641	26	-1.8586659	MD03-2641	33.3	-0.96433375
MD03-2641	21.4	-0.84067783	MD03-2641	26.1	-1.5561528	MD03-2641	33.6	-2.0819721
MD03-2641	21.5	-0.86189429	MD03-2641	26.3	-1.4666065	MD03-2641	33.8	-2.1552662
MD03-2641	21.6	-0.23297799	MD03-2641	26.4	-2.0993718	MD03-2641	34	-2.2301146
MD03-2641	21.7	-0.40039769	MD03-2641	26.5	-2.0934316	MD03-2641	34.1	-2.6626459
MD03-2641	21.8	-0.71736315	MD03-2641	26.6	-2.2681576	MD03-2641	34.3	-2.5047177
MD03-2641	21.9	-1.3125396	MD03-2641	26.7	-2.3462438	MD03-2641	34.4	-1.0971849
MD03-2641	22	-0.88581566	MD03-2641	26.8	-2.5786626	MD03-2641	34.6	-2.0688598
MD03-2641	22.1	-0.28473214	MD03-2641	27.1	-3.0520096	MD03-2641	35	-1.7680453
MD03-2641	22.2	-1.6587706	MD03-2641	27.6	-2.2321963	MD03-2641	35.7	-1.2173545
MD03-2641	22.3	-1.0526049	MD03-2641	27.7	-3.0639633	MD03-2641	35.8	-2.1597485
MD03-2641	22.4	-0.68861697	MD03-2641	28.6	-2.8769722	MD03-2641	35.9	-3.2352328
MD03-2641	22.5	-0.8806021	MD03-2641	28.7	-3.2832354	MD03-2641	35.9	-1.7340082
MD03-2641	22.6	-1.4217253	MD03-2641	28.9	-2.3206784	MD03-2641	36.7	-2.519314
MD03-2641	22.7	-0.92122159	MD03-2641	29	-2.516779	MD03-2641	36.8	-2.0375383
MD03-2641	22.8	-1.429892	MD03-2641	29.1	-2.4405908	MD03-2641	36.9	-1.8525775
MD03-2641	22.9	-1.3497555	MD03-2641	29.6	-2.4160597	MD03-2641	37	-1.1914902
MD03-2641	23	-1.7022256	MD03-2641	29.9	-2.2821593	MD03-2641	37.4	-0.19412499
MD03-2641	23.1	-1.9584638	MD03-2641	30	-2.4171704	MD03-2641	37.8	-0.71301863
MD03-2641	23.2	-2.2950303	MD03-2641	30.1	-2.1914121	MD03-2641	38	-0.82075617
MD03-2641	23.3	-2.8584966	MD03-2641	30.2	-1.9190162	MD03-2641	38.2	-0.057981358
MD03-2641	23.4	-2.5837839	MD03-2641	30.4	-1.6763493	MD03-2641	38.4	-1.3185424
MD03-2641	23.5	-2.3222856	MD03-2641	30.5	-1.2061886	MD03-2641	38.6	-0.076920746
MD03-2641	23.6	-2.4495429	MD03-2641	30.6	-1.4149815	MD03-2641	38.7	-0.24119682
MD03-2641	23.7	-2.1919529	MD03-2641	30.7	-1.5993678	MD03-2641	38.8	-0.58666173
MD03-2641	23.8	-1.9364364	MD03-2641	30.8	-1.5873462	MD03-2641	39.1	0.002667473
MD03-2641	23.9	-1.0591259	MD03-2641	30.9	-1.8428415	MD03-2641	39.2	-0.30211574
MD03-2641	24	-1.820406	MD03-2641	31	-1.9715698	MD03-2641	39.4	-0.16397326
MD03-2641	24.1	-2.4236125	MD03-2641	31.1	-1.4578448			
MD03-2641	24.2	-2.1659368	MD03-2641	31.2	-2.2138917			
MD03-2641	24.3	-1.4180794	MD03-2641	31.3	-2.3262918			
MD03-2641	24.4	-1.6805595	MD03-2641	31.4	-1.8762751			
MD03-2641	24.5	-1.3363933	MD03-2641	31.5	-2.7484348			
MD03-2641	24.6	-1.2969437	MD03-2641	31.6	-2.9081961			
MD03-2641	24.7	-1.0554105	MD03-2641	31.7	-2.313039			
MD03-2641	24.8	-1.2574541	MD03-2641	31.8	-3.2443008			
MD03-2641	24.9	-1.4331907	MD03-2641	31.9	-2.9848125			
MD03-2641	25	-1.3159272	MD03-2641	32	-2.9474395			

Appendix B: Mg/Ca Data

Table B.1. Mg/Ca Data for Hole 1319A

Core IODP-1319A Species: *G. ruber* Size Specimen: 150-250 μm

Location: 27°15.9751'N 94°24.190'W

General remarks: Lots of iron but Mg/Ca still in agreement with *G. ruber* $\delta^{18}\text{O}$ data

Depth (mbsf)	Mg/Ca (mmol/mol)	Sr/Ca (mmol/mol)	Al/Ca (mmol/mol)	Fe/Ca (mmol/mol)	Fe/Mg (mol/mol)	Mn/Ca (mmol/mol)	Mn/Fe (mol/mol)	SST temp °C	$\delta^{18}\text{O}$	$\delta^{18}\text{O}_{\text{SW}}$ (VSMOW)
27.44	4.895	1.481	0.129	0.264	0.055	0.783	2.969	28.39	-3.23	-0.153
27.81	4.259	1.518	0.115	0.105	0.025	0.723	6.869	26.85	-1.27	1.488
29.53	4.386	1.479	0.143	0.274	0.064	1.674	6.106	27.17	-1.31	1.516
30.13	4.883	1.468	0.112	0.369	0.077	2.116	5.738	28.36	-2.13	0.939
30.84	4.990	1.477	0.110	0.268	0.055	1.046	3.906	28.61	-3.72	-0.594
31.06	4.637	1.452	0.119	0.261	0.057	0.957	3.663	27.79	-3.08	-0.131
31.33	4.571	1.473	0.108	0.220	0.049	0.655	2.985	27.63	-2.34	0.583
31.56	4.034	1.460	0.123	0.343	0.087	0.713	2.077	26.24	-2.67	-0.045
31.67	5.815	1.437	0.130	0.294	0.051	0.560	1.901	30.31	-2.601	0.879
31.93	5.457	1.460	0.118	0.251	0.047	0.506	2.013	29.60	-2.33	1.001
32.24	4.769	1.467	0.099	0.675	0.145	0.434	0.643	28.10	-2.13	0.885
32.83	4.502	1.454	0.127	0.626	0.143	0.615	0.983	27.46	-2.50	0.384
33.52	3.576	1.449	0.112	0.599	0.173	0.582	0.971	24.90	-1.42	0.931
35.02	4.122	1.464	0.060	0.574	0.142	0.378	0.658	26.48	-1.46	1.223
35.83	3.763	1.446	0.104	0.719	0.197	0.473	0.658	25.47	-1.00	1.468
36.65	3.431	1.453	0.119	0.763	0.230	0.345	0.452	24.45	-0.60	1.652
37.28	3.740	1.443	0.124	0.660	0.182	0.580	0.879	25.40	-0.85	1.604
38.14	3.925	1.435	0.124	0.654	0.171	0.388	0.593	25.94	-0.86	1.706
38.83	3.381	1.439	0.108	0.608	0.186	0.499	0.821	24.28	-1.03	1.195
39.58	4.216	1.459	0.072	0.727	0.176	0.398	0.548	26.73	-1.93	0.802
40.33	4.004	1.508	0.081	0.888	0.227	0.416	0.468	26.16	-1.59	1.021
41.08	3.776	1.455	0.106	0.740	0.201	0.393	0.531	25.51	-1.58	0.900
42.52	3.807	1.478		0.818	0.220	0.215	0.263	25.60	-1.40	1.093
43.84	3.446	1.447		0.778	0.226	0.152	0.195	24.49	-1.29	0.976
44.57	3.158	1.439	0.161	0.933	0.298	0.220	0.236	23.52	-1.21	0.849
45.32	3.416	1.456	0.138	0.766	0.226	0.212	0.277	24.40	-1.04	1.207
47.56	3.454	1.479	0.056	0.786	0.234	0.307	0.390	24.52		
48.31	4.344	1.475	0.066	0.761	0.179	0.143	0.188	27.07	-1.44	1.362
49.84	3.686	1.446	0.091	0.853	0.237	0.308	0.361	25.24	-1.69	0.733
50.58	3.412	1.494		0.697	0.210	0.224	0.321	24.38	-1.24	1.006
52.03	3.220	1.464	0.147	0.843	0.264	0.195	0.231	23.74	-5.07	1.6051
52.58	3.893	1.451	0.116	0.704	0.183	0.170	0.242	25.85	-1.72	0.824
55.15	4.272	1.485	0.078	0.788	0.188	0.289	0.367	26.88	-1.40	1.358
55.58	4.332	1.457	0.117	0.897	0.211	0.185	0.206	27.043	-2.11	0.681
56.31	3.728	1.484	0.067	0.728	0.200	0.202	0.278	25.371	-0.35	2.092

Depth (mbsf)	Mg/Ca (mmol/ mol)	Sr/Ca (mmol/ mol)	Al/Ca mmol/ mol	Fe/Ca mmol/ mol	Fe/Mg mol/mol	Mn/Ca mmol/ mol	Mn/Fe mol/ mol	SST temp °C	$\delta^{18}\text{O}$	$\delta^{18}\text{O}_{\text{sw}}$ (VSMOW)
58.57	3.785	1.480	0.086	0.766	0.204	0.184	0.240	25.544	-0.84	1.642
59.32	3.338	1.453	0.137	0.746	0.226	0.169	0.227	24.14	-1.69	0.496
60.09	3.449	1.469	0.102	0.677	0.198	0.121	0.178	24.50	-0.70	1.567
61.54	3.692	1.483	0.066	0.657	0.183	0.100	0.151	25.263	-2.27	0.1499
62.08	3.984	1.467		0.940	0.241	0.131	0.139	26.11	-1.48	1.124
63.58	3.827	1.471		0.868	0.232	0.151	0.174	25.66	-1.50	1.01
64.31	3.609	1.445	0.135	0.679	0.190	0.103	0.152	25.013	-1.02	1.34
64.65	3.525	1.458	0.144	0.677	0.194	0.091	0.134	24.75	-1.12	1.202
65.08	3.351	1.463	0.131	0.642	0.193	0.090	0.140	24.18	-0.68	1.520
65.81	3.711	1.462	0.117	0.625	0.170	0.099	0.159	25.32	-1.26	1.17
68.86	4.254	1.520	0.068	0.602	0.144	0.101	0.168	26.83	-1.21	1.545
69.58	3.720	1.478	0.087	0.659	0.182	0.090	0.137	25.34	-0.60	1.8379
70.33	3.478	1.460	0.078	0.670	0.198	0.102	0.152	24.60	-1.36	0.928
71.07	3.687	1.451	0.108	0.719	0.197	0.096	0.134	25.24	-2.02	0.397
71.6	4.025	1.466	0.095	0.690	0.173	0.115	0.167	26.22	-1.67	0.953
72.31	4.141	1.458	0.117	0.654	0.159	0.081	0.124	26.53	-1.40	1.292
74.14	3.522	1.454	0.092	0.602	0.173	0.067	0.111	24.73	-1.16	1.153
76.79	4.004	1.500	0.104	0.681	0.174	0.155	0.228	26.16	-1.05	1.558
77.59	4.360	1.491	0.092	0.746	0.174	0.146	0.195	27.11	-1.49	1.324
78.34	3.635	1.494		0.666	0.188	0.149	0.224	25.09	-0.99	1.393
79.09	3.265	1.463	0.142	0.784	0.242	0.248	0.316	23.89	-1.09	1.05
79.6	2.955	1.444	0.114	0.791	0.270	0.226	0.286	22.785	-1.15	0.754
80.52	3.139	1.472	0.112	0.902	0.290	0.403	0.446	23.46	-1.07	0.974
81.09	3.254	1.466	0.170	0.733	0.227	0.611	0.835	23.85	-1.38	0.752
84.8	4.814	1.514	0.094	0.602	0.127	0.200	0.332	28.21	-1.03	2.004
85.57	3.862	1.511	0.085	0.697	0.185	0.157	0.225	25.76	-0.56	1.968
86.4	3.961	1.522	0.079	0.581	0.150	0.197	0.339	26.04	-0.77	1.8142
87.1	3.341	1.475	0.109	0.639	0.193	0.231	0.361	24.15	-1.19	1.007
87.67	3.415	1.477	0.109	0.589	0.174	0.240	0.408	24.39	-1.01	1.233
88.57	3.606	1.470	0.120	0.561	0.157	0.207	0.369	25.003	-0.88	1.485
89.99	3.920	1.424	0.131	0.530	0.136	0.202	0.382	25.928	-2.35	0.208
92.2	5.342	1.515	0.173	0.784	0.148	0.278	0.354	29.36	-0.93	2.347
92.95	3.909	1.520		0.538	0.141	0.073	0.135	25.89	-1.08	1.472
93.7	4.151	1.479	0.069	0.611	0.150	0.246	0.403	26.56	-2.03	0.668
94.45	4.118	1.506	0.121	0.632	0.155	0.078	0.123	26.47	-0.62	2.055
95.19	4.051	1.492		0.647	0.160	0.113	0.175	26.29	-1.24	1.39
95.94	4.137	1.490	0.119	0.562	0.137	0.117	0.209	26.52	-1.20	1.48
96.7	3.894	1.506	0.086	0.584	0.151	0.107	0.183	25.85	-0.51	2.032

Appendix C: Additional Figures

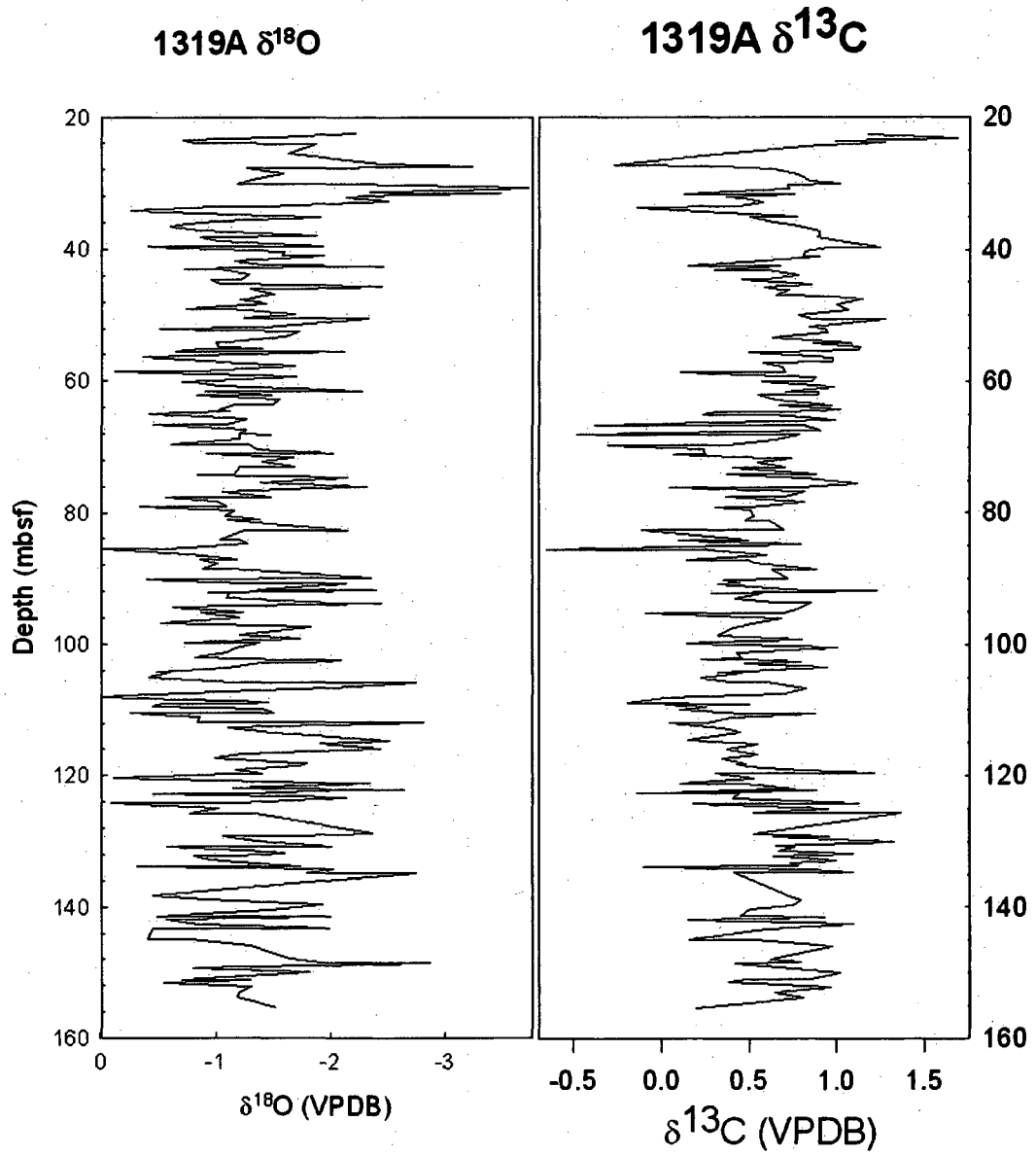


Figure C.1. Comparison of $\delta^{18}\text{O}$ and $\delta^{13}\text{C}$ from Hole 1319A.

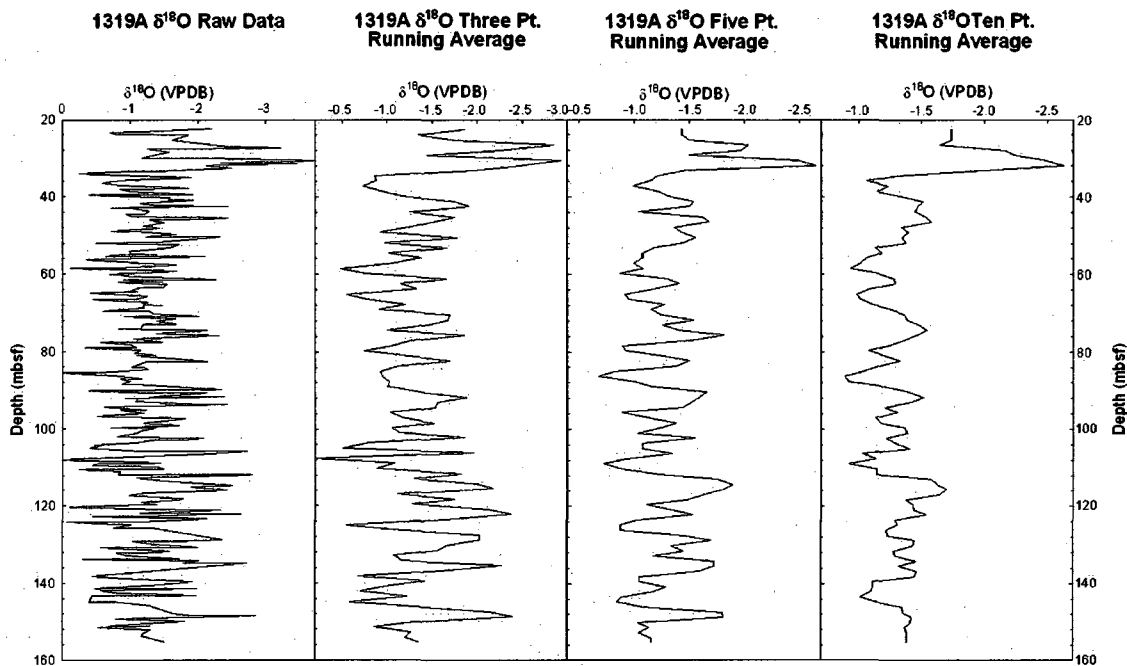


Figure C.2. $\delta^{18}\text{O}$ data for Hole 1319A versus a variety of running averages. The five point moving average was used for this study.

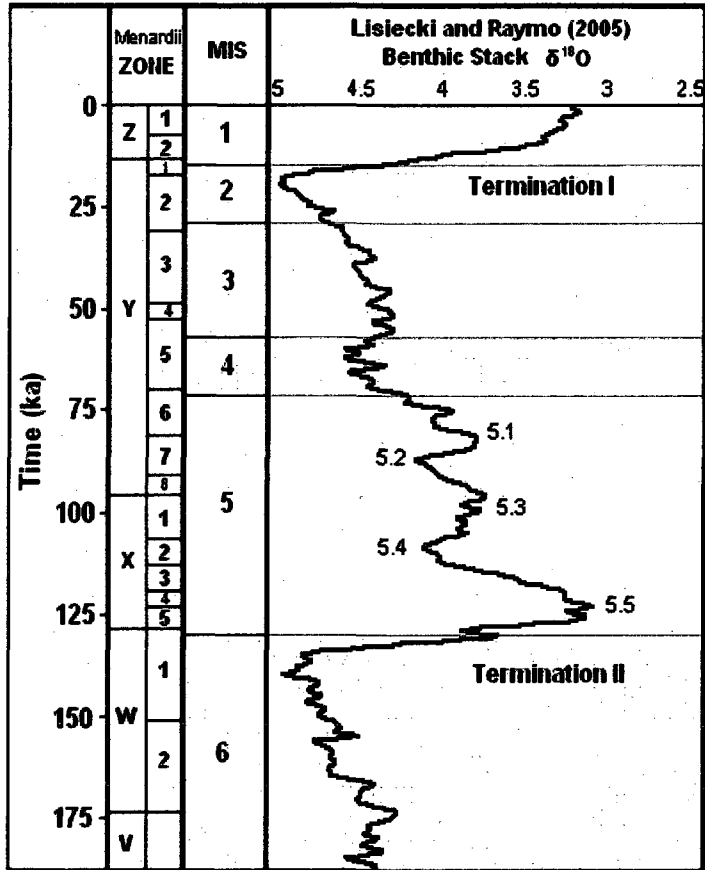


Figure C.3. A combination diagram showing the global benthic $\delta^{18}\text{O}$ stack (Lisiecki and Raymo, 2005), with corresponding Marine Isotope Stages, and *G. menardii* zones for the Gulf of Mexico (Kennett and Huddlestun, 1972).

